arXiv:1510.07018v2 [hep-th] 20 May 2016

Asymptotic safety of gravity-matter systems

J. Meibohm,[1] J. M. Pawlowski,[1,2] and M. Reichert[1]

[1] *Institut für Theoretische Physik, Universität Heidelberg, Philosophenweg 16, 69120 Heidelberg, Germany*
[2] *ExtreMe Matter Institute EMMI, GSI Helmholtzzentrum für Schwerionenforschung mbH, Planckstr. 1, 64291 Darmstadt, Germany*

We study the ultraviolet stability of gravity-matter systems for general numbers of minimally coupled scalars and fermions. This is done within the functional renormalisation group setup put forward in [1] for pure gravity. It includes full dynamical propagators and a genuine dynamical Newton's coupling, which is extracted from the graviton three-point function.

We find ultraviolet stability of general gravity-fermion systems. Gravity-scalar systems are also found to be ultraviolet stable within validity bounds for the chosen generic class of regulators, based on the size of the anomalous dimension. Remarkably, the ultraviolet fixed points for the dynamical couplings are found to be significantly different from those of their associated background counterparts, once matter fields are included. In summary, the asymptotic safety scenario does not put constraints on the matter content of the theory within the validity bounds for the chosen generic class of regulators.

I. INTRODUCTION

The asymptotic safety scenario proposed by S. Weinberg [2] almost 40 years ago has received growing attention in the last decades. It provides a promising route towards the formulation of quantum gravity as a non-perturbatively renormalisable quantum field theory of the metric. In terms of the renormalisation group, the asymptotic safety scenario conjectures the existence of a non-trivial ultraviolet (UV) fixed point of the renormalisation group flow.

The development of modern functional renormalisation group (FRG) techniques and their application to quantum gravity [3, 4] has led to strong evidence for the non-trivial UV fixed point for pure gravity. It was first found in basic Einstein-Hilbert approximations [3, 5, 6] and later confirmed in more elaborate truncations [1, 7–24], for reviews see [25–28].

One of the most interesting open physics questions concerns the UV completions of the Standard Model of particle physics. This requires the investigation of the UV stability of interacting gravity-matter systems, and in particular those with large numbers of matter fields. First interesting results and developments in this direction have been obtained in [29–36]. An interacting fixed point in gravity-matter systems requires a non-trivial interplay of the fluctuation dynamics of all involved fields. In other theories it is well-known, that the inclusion of additional fields may change the nature of the theory. For example, in QCD with many quark flavours asymptotic freedom is lost, thus rendering the UV-limit of the theory ill-defined for a large number of quarks. Analogously, matter fields could potentially spoil asymptotic safety in combined systems of gravity and matter. This has indeed been observed in [30] in the background field approximation and in [34, 35] with a mixed approach, where the background field approximation for the couplings is augmented with dynamical anomalous dimensions. In the background field approximation no distinction is made between dynamical and background fields. However, the differences between these fields are potentially of qualitative nature, see [32, 37–41]. More recently, a more careful treatment of background and dynamical fluctuating fields has been provided by, e.g., the FRG setup with dynamical correlation functions in [1, 7, 8], the use of the geometrical effective action and the corresponding Nielsen identities [9, 40–45], or bi-metric approaches [46, 47].

In this work we analyse the influence of scalar and fermionic matter on the non-trivial UV fixed point of quantum gravity in the dynamical FRG setup put forward in [1]. The matter contributions to the quantum gravity system are extracted, for the first time, from the higher order dynamical correlation functions in the framework of the FRG. As introduced in [1, 7, 8] we analyse a system of vertex flows evaluated at flat Euclidean background. We also introduce a validity bound on the generic class of regulators used here, based on the size of the anomalous dimensions. This regime includes an arbitrary numbers of fermions, whereas it restricts the number of allowed scalars that can be discussed with the present generic class of regulators to a maximum $\lesssim 20$. Within this regime of validity we find that the UV-fixed point persists and remains UV stable. We also find that the UV fixed points for the dynamical couplings are significantly different from those of their associated background counterparts, once matter fields are included. In summary, the asymptotic safety scenario does not put constraints on the matter content of the theory within the validity bounds for the chosen generic class of regulators.

II. FUNCTIONAL RENORMALISATION GROUP

The basic quantity in the functional renormalisation group approach [4, 48–50] is the quantum effective action $\Gamma[\bar{g}, \phi]$, where ϕ is a superfield containing the dynamical fields of the theory and $\bar{g}_{\mu\nu}$ is the background metric.

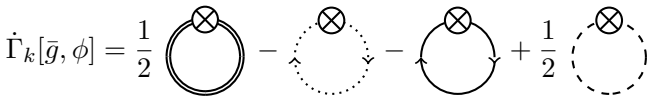

FIG. 1. Flow equation for the scale dependent effective action Γ_k in diagrammatic representation. The double, dotted, solid and dashed lines correspond to the graviton, ghost, fermion and scalar propagators, respectively. The crossed circles denote the respective regulator insertions.

For our set of fields, ϕ reads

$$\phi = (h, c, \bar{c}, \psi_i, \bar{\psi}_j, \varphi_l)\,, \tag{1}$$

where $h_{\alpha\beta}$ and $(\bar{c}_\mu, c_\nu)$ are the fluctuating graviton and the (anti-) ghost fields, respectively. The fermion fields $(\bar{\psi}_i, \psi_j)$, carrying the flavour indices $i, j \in 1 \dots N_f$, and the real scalars φ_l of flavour $l = 1 \dots N_s$ constitute the matter contributions to ϕ.

The scale dependent effective action $\Gamma_k[\bar{g}, \phi]$ is formally defined by introducing k-dependent IR regulators R_k^ϕ for the fluctuation fields ϕ on the level of the path integral. We call the scale parameter k the renormalisation scale. The regulators are quadratic in the fluctuating fields, which requires to introduce a background metric $\bar{g}_{\mu\nu}$ for metric theories of gravity. The physical (full) metric $g_{\mu\nu}$ is given by a linear split between background metric $\bar{g}_{\mu\nu}$ and the fluctuation field $h_{\mu\nu}$ according to $g_{\mu\nu} = \bar{g}_{\mu\nu} + h_{\mu\nu}$. The scale dependent effective action $\Gamma_k[\bar{g}, \phi]$ obeys a one-loop flow equation. For the given field content ϕ the latter reads

$$\begin{aligned}\dot{\Gamma}_k =& \frac{1}{2}\,\mathrm{Tr}\left[\frac{1}{\Gamma_k^{(2)} + R_k}\dot{R}_k\right]_{hh} - \mathrm{Tr}\left[\frac{1}{\Gamma_k^{(2)} + R_k}\dot{R}_k\right]_{\bar{c}c} \\ &- \mathrm{Tr}\left[\frac{1}{\Gamma_k^{(2)} + R_k}\dot{R}_k\right]_{\bar{\psi}\psi} + \frac{1}{2}\,\mathrm{Tr}\left[\frac{1}{\Gamma_k^{(2)} + R_k}\dot{R}_k\right]_{\phi\phi}\,.\end{aligned} \tag{2}$$

Here we have introduced the notation $\dot{f} = \partial_t f$ where $t = \ln(\frac{k}{k_0})$ is the renormalisation time with some reference scale k_0. Figure 1 depicts equation (2) in terms of diagrams. Since (2) is not solvable in general, $\Gamma_k[\bar{g}, \phi]$ is truncated to a finite dimensional set of operators. In our approach, the latter set is given by the n-point correlation functions $\Gamma_k^{(hh)}$, $\Gamma_k^{(hhh)}$, $\Gamma_k^{(\bar{\psi}\psi)}$ and $\Gamma_k^{(\phi\phi)}$, where we employ the condensed notation for the k-dependent 1 PI n-point functions

$$\Gamma_k^{(\phi_1 \dots \phi_n)}[\bar{g}, \phi] := \frac{\delta^n \Gamma_k[\bar{g}, \phi]}{\delta\phi_1 \dots \delta\phi_n}\,. \tag{3}$$

The flow equations for this set of operators are obtained by taking field variations of the flow equation (2) and expanding the full scale dependent effective action in powers of the fields according to

$$\begin{aligned}\Gamma_k[\bar{g}, \phi] =& \sum_{n=0}^{\infty} \frac{1}{n!}\Gamma_k^{(\phi_1 \dots \phi_n)}[\bar{g}, 0]\phi_1 \cdots \phi_n \\ =& \Gamma_k[\bar{g}, 0] + \Gamma_k^{(h)}[\bar{g}, 0]h + \frac{1}{2}\Gamma_k^{(2h)}[\bar{g}, 0]h^2 \\ &+ \frac{1}{3!}\Gamma_k^{(3h)}[\bar{g}, 0]h^3 + \frac{1}{2}\Gamma_k^{(\bar{c}c)}[\bar{g}, 0]\bar{c}\,c \\ &+ \frac{1}{2}\Gamma_k^{(\bar{\psi}\psi)}[\bar{g}, 0]\bar{\psi}\,\psi + \frac{1}{2}\Gamma_k^{(\varphi\varphi)}[\bar{g}, 0]\varphi^2 + \dots\,.\end{aligned} \tag{4}$$

This vertex expansion of the scale dependent effective action was introduced in [1, 7, 8] in the context of pure quantum gravity. In other related works, anomalous dimensions were computed with vertex expansions on a flat background and were used in combination with the background-field approach [20, 34, 51]. Together with [1], however, the present work is the first minimally self-consistent analysis of such vertex flows in quantum gravity.

Note that $\Gamma_k[\bar{g}, \phi]$ in (4) is expanded about an, a priori, arbitrary fixed metric background $\bar{g}_{\mu\nu}$. As we will see, however, the present setup allows us to evaluate all relevant flow parameters on a flat Euclidean background, i.e. $\bar{g}_{\mu\nu} = \delta_{\mu\nu}$. In (4), the zero-point function $\Gamma_k[\bar{g}, 0]$ and the one-point function $\Gamma_k^{(h)}[\bar{g}, 0]$ are non-dynamical (background-) quantities that do not feed back into the flow of the dynamical n-point functions. Therefore we first focus on the computation of the latter ones and afterwards, in section V, use the solution of the dynamical couplings for a self-consistent computation of the background couplings. Since the right hand side of the flow equation (2) contains second variations of the fields, the flows for the respective n-point functions contain n-point vertices up to order $n + 2$. More precisely, the present setup requires the evaluation of vertices with up to five fields.

We also want to briefly compare the present expansion scheme with the standard heat kernel expansion in the background field approximation. In this approximation it is assumed that the scale dependent effective action is a functional of only one single metric field $g = \bar{g} + h$. Note that this approximation has the seeming benefit of a diffeomorphism invariant expansion scheme and a closed, diffeomorphism invariant effective action. However, the background field approximation does not satisfy the non-trivial Slavnov-Taylor identities for the dynamical metric h as well as the Nielsen identity, that link $\bar{g}$-dependences and h-dependences, see in particular [9, 32, 40, 41, 43–45]. Hence, while based on a diffeomorphism-invariant effective action, the background field approximation is at odds with diffeomorphism invariance for this very reason. Note that this also implies that background independence is at stake. The potential severeness of the related problems has been illustrated early on at the simpler example of a non-Abelian gauge theory in [38]. These problems can either be resolved in the present approach within a flat background expansion, the geometrical effective action approach, see [9, 40–42]. or in the bi-metric approach, see [46, 47]. Results within these

approaches also allow for a systematic check of the reliability of the background field approximation. Note also that the full resolution of the background independcence within the bi-metric approach requires the computation of h-correlation function functions of the order two and higher as it is only these correlation functions that enter the flow equation on the right hand side. So far, this has not been undertaken.

The heat kernel computation expands the solution in powers of the Ricci scalar R, to wit

$$\dot{\Gamma}_k[g] = c_0 \int d^4x\,\sqrt{g} + c_1 \int d^4x\,\sqrt{g}\,R + \mathcal{O}(R^2)\,. \tag{5}$$

The coefficients $c_0 = c_0(\dot{\bar{g}}, \dot{\bar{\lambda}})$ and $c_1 = c_1(\dot{\bar{g}}, \dot{\bar{\lambda}})$ are related to flow of the background couplings. By computing the flow for the graviton two-point function for this hypothetical situation according to

$$\mathcal{F} \circ \dot{\Gamma}_k^{(2h)}[\bar{g}]\Big|_{\bar{g}=\delta} = c_0 \mathcal{T}^{(2h)}(0) + c_1 \mathcal{T}^{(2h)}(\mathbf{p})\,, \tag{6}$$

where $\mathcal{F}$ denotes the Fourier transform, we observe that the coefficients c_0 and c_1 are obtained analogously from the momentum independent and momentum dependent parts of the graviton two-point function, respectively. The tensor structures $\mathcal{T}$ are defined later in (9). In consequence, we extract exactly the same information from the flow within the flat vertex expansion that is obtained in the heat kernel approach. In case of higher order operators, we are even able to distinguish between the flows of e.g. R^2 and $R_{\mu\nu}R^{\mu\nu}$. Considering the realistic situation that the flow is not a functional of only one single metric but of a background and a fluctuating field, the vertex expansion further conveniently disentangles the flows of their corresponding couplings. In summary the present approach retains the results of standard heat kernel computation although it is evaluated on a flat background but has significant advantages in the non-single metric of quantum gravity.

In order to obtain running couplings from the flow of the n-point functions we employ a vertex dressing according to

$$\Gamma_k^{(\phi_1\dots\phi_n)} = \sqrt{\prod_{i=1}^{n} Z_{\phi_i}(p_i^2)\, G_n^{\frac{n}{2}-1}}\,\mathcal{T}^{(\phi_1\dots\phi_n)}\,, \tag{7}$$

where Z_{ϕ_i} denote the wavefunction renormalisations of the respective fields in ϕ which are functions of the field momenta p_i^2. $\mathcal{T}^{(\phi_1\dots\phi_n)}$ is the tensor structure of the respective vertex and shall be defined in (9). In general, we assign to any n-vertex an individual, momentum dependent Newton's constant $G_n(\mathbf{p})$, with $\mathbf{p} = (p_1, \dots, p_n)$. In this work, however, we approximate all G_n as one, momentum-independent coupling, $G_n(\mathbf{p}) \equiv G_3 =: G$. Note, that Z_ϕ and G are scale dependent, although we drop the subscript k here and in the following for notational convenience. In Figure 2 the vertex dressing of all involved the three-point vertices are given according to (7). Generalisations to higher order vertices can be inferred from (7). Note, that (7) suggests an expansion in rescaled fields $\bar{\phi}$ and rescaled vertices $\bar{\Gamma}^{(\phi_1\dots\phi_n)}$ with

$$\phi = \frac{\bar{\phi}}{\sqrt{Z_\phi}}\,, \qquad \bar{\Gamma}^{(\phi_1\dots\phi_n)} = \frac{\Gamma^{(\phi_1\dots\phi_n)}}{\sqrt{\prod_{i=1}^{n} Z_{\phi_i}(p_i^2)}} \simeq G_n^{\frac{n}{2}-1}\,, \tag{8}$$

see also [8, 41, 52]. Such a rescaling absorbs the RG-running of the vertices in the fields, and hence is an expansion in RG-invariant, but cutoff-dependent, quantities, for more details on this aspect see [8, 41, 52]. The underlying structure is elucidated by the kinetic term $\bar{\Gamma}^{(\phi_1\phi_2)}$: it has the classical form without wave function renormalisation, and hence does not scale under RG-transformations. This discussion highlights the rôle of the couplings G_n as RG-invariant running couplings.

The tensor structures $\mathcal{T}$ are given by variations of the classical action S with respect to the fluctuation fields. More precisely, the latter read

$$\mathcal{T}^{(\phi_1\dots\phi_n)}(\mathbf{p}; \Lambda_n) = S^{(\phi_1\dots\phi_n)}(\mathbf{p}; \Lambda \to \Lambda_n, G_N \to 1)\,. \tag{9}$$

In (9) the classical action S is given by the Einstein-Hilbert action added by covariant fermion and scalar kinetic terms according to

$$S = S_{\rm EH} + \int \mathrm{d}^4x\sqrt{g}\bar{\psi}_i \not{\nabla}\psi_i + \frac{1}{2}\int \mathrm{d}^4x\sqrt{g}g_{\mu\nu}\partial^\mu\varphi_l\partial^\nu\varphi_l\,, \tag{10}$$

where we used the conventional slash-notation for the contraction of the spin-covariant derivative ∇^μ with gamma matrices. The covariant kinetic terms for the matter fields in (10) lead to minimal coupling between gravity and matter in the present truncation. For the formulation of fermions in curved spacetime we use the the spin-base invariance formalism introduced in [53–55]. This allows to circumvent possible ambiguities arising in the vielbein formalism and relies on spacetime dependent γ-matrices and the spin-connection Γ^μ. As a result, $\not{\nabla}$ reads

$$\not{\nabla} = g_{\mu\nu}\gamma(x)^\mu\nabla^\nu = g_{\mu\nu}\gamma(x)^\mu(\partial^\nu + \Gamma(x)^\nu)\,, \tag{11}$$

if it acts on a spinor as in (10). In the following, we drop the explicit spacetime dependence of the latter quantities for a more convenient notation. The gauge-fixed Einstein-Hilbert action $S_{\rm EH}$ in (10) reads

$$S_{\rm EH} = \frac{1}{16\pi G_N}\int \mathrm{d}^4x\sqrt{g}(2\Lambda - R) + S_{\rm gf} + S_{\rm gh}\,, \tag{12}$$

where Λ denotes the classical cosmological constant and R is the curvature scalar. The terms $S_{\rm gf}$ and $S_{\rm gh}$ are the gauge fixing and the Faddeev-Popov-ghost action, respectively. Both latter contributions are determined by the gauge condition F_μ. The gauge fixing action reads

$$S_{\rm gf} = \frac{1}{32\pi\alpha}\int \mathrm{d}^4x\sqrt{\bar{g}}\,\bar{g}^{\mu\nu}F_\mu F_\nu\,. \tag{13}$$

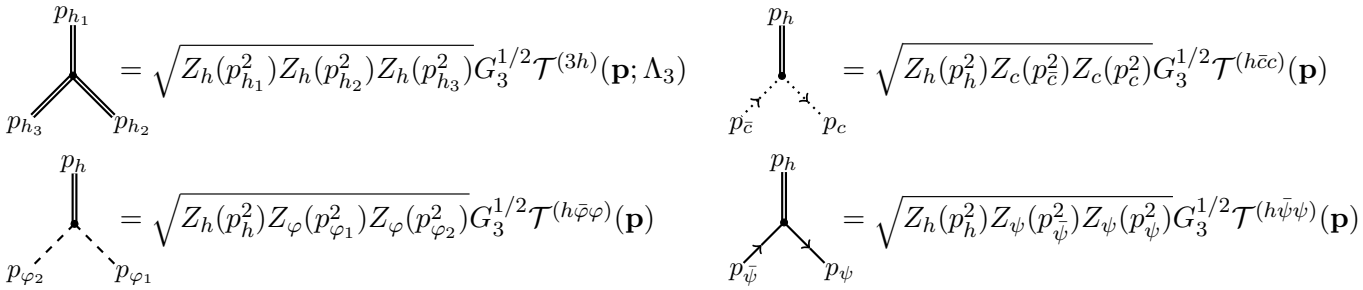

FIG. 2. Vertex dressing of all three-point vertices used in this work. The vertex dressing consist of the respective wave function renormalisations, couplings and tensor structures. The first line in the figure depicts all pure gravity three-point vertices while the second line shows the ones with gravity-matter-interactions.

In this work, we apply a De-Donder-type linear gauge given by

$$F_\mu = \bar{\nabla}^\nu h_{\mu\nu} - \frac{1+\beta}{4}\bar{\nabla}_\mu h^\nu{}_\nu \,, \tag{14}$$

with $\beta = 1$. Furthermore, we apply the Landau-limit of vanishing gauge parameter, $\alpha \to 0$. The Faddeev-Popov operator corresponding to (14) is of the form

$$\mathcal{M}_{\mu\nu} = \bar{\nabla}^\rho \left(g_{\mu\nu}\nabla_\rho + g_{\rho\nu}\nabla_\mu\right) - \bar{\nabla}_\mu\nabla_\nu \,. \tag{15}$$

The Landau-limit $\alpha \to 0$ is particularly convenient since it provides a sharp implementation of the gauge fixing. This assures furthermore, that the corresponding gauge-fixing parameter is at a fixed point of the renormalisation group flow [56].

The vertex flows discussed here carry additional spacetime and momentum indices. In order to obtain scalar flow equations for the couplings the appropriate projection of the flows is a crucial part of the present truncation and goes along the same lines as in [1]. It can be summed up in a three step procedure:

(i) We decompose $\mathcal{T}^{(n_h)}$, where n_h is the number of variations with respect to h, into its momentum dependent and momentum independent part according to

$$\mathcal{T}^{(n_h)}(\mathbf{p};\Lambda_{n_h}) = \mathcal{T}^{(n_h)}(\mathbf{p};0) + \Lambda_{n_h}\mathcal{T}^{(n_h)}(0;1) \,. \tag{16}$$

In (16), the first term on the right-hand side is quadratic in the external graviton momenta $\mathbf{p}$ for the current truncation. The second term is momentum independent.

(ii) From (16) we take the dimensionless tensors $\mathcal{T}^{(n_h)}(\mathbf{p};0)/\mathbf{p}^2$ and $\mathcal{T}^{(n_h)}(0;1)$ and separately multiply all spacetime-index pairs of both tensors with transverse-traceless projection operators Π_{TT}. This leaves us with the two tensors $\mathcal{T}^{(n_h)}_{\text{TT}}(\mathbf{p};0)/\mathbf{p}^2$ and $\mathcal{T}^{(n_h)}_{\text{TT}}(0;1)$, each of them carries $2n_h$ spacetime indices.

(iii) We contract the left and the right hand side of the vertex flow with these two tensors, in order to obtain Lorentz-scalar expressions. Hereby, the tensors $\mathcal{T}^{(n_h)}_{\text{TT}}(\mathbf{p};0)/\mathbf{p}^2$ and $\mathcal{T}^{(n_h)}_{\text{TT}}(0;1)$ are used to project the tensorial flow onto the scalar flows of G_{n_h} and Λ_{n_h}, respectively.

The projection operators are detailed in Appendix A. In addition to the spacetime indices, the vertex flows carry spinor, flavour and colour indices. These however, can be trivially traced out after multiplying appropriately with γ and $\mathbb{1}$-matrices.

After having traced out all discrete indices the resulting flow still depends on the external field momenta $\mathbf{p}$. This dependence is dealt with by choosing a specific kinematic configuration. Since all vertices obey momentum conservation this choice is only relevant for n-point vertices with $n \geq 3$. In this work, the flow of the graviton three-point function is the highest order vertex flow and thus it is the only flow that needs a fixed kinematic configuration. For the latter, we choose the maximally symmetric configuration, to wit

$$|p_1| = |p_2| =: p \,, \qquad \vartheta = 2\pi/3 \,, \tag{17}$$

where ϑ is the angle between p_1 and p_2. Note, that p_3 was eliminated using momentum conservation. This way, both sides of the flow equations for all vertices only depend on the scalar momentum parameter p. Note, that due to the vertex construction (7) and the choice of regulators R_k^ϕ to be specified below there are no single wave-function renormalisations Z_{ϕ_i} in the flow. Instead, the latter always enter in terms of the corresponding anomalous dimensions η_{ϕ_i} defined by

$$\eta_{\phi_i}(p^2) := -\partial_t \ln Z_{\phi_i}(p^2) \,. \tag{18}$$

Consequently, the flow of a generic ϕ^n-vertex reads schematically

$$\text{Flow}^{(\phi^n)} = \int_q \left(\dot{r}_{\phi_i}(q^2) - \eta_{\phi_i}(q^2) r_{\phi_i}(q^2)\right) F_i^{(\phi^n)}(p, q, \dots) \,, \tag{19}$$

where we have defined $\mathrm{Flow}^{(\phi^n)}$ as

$$\mathrm{Flow}^{(\phi^n)}(p^2) := \frac{\dot{\Gamma}^{(\phi_1\dots\phi_n)}(p^2)}{\prod_{i=1}^n \sqrt{Z_{\phi_i}(p^2)}}\,. \tag{20}$$

In (19), r_{ϕ_i} denotes the regulator shape function corresponding to the field ϕ_i and the functions $F_i^{(\phi^n)}$ encode the contributions of the field ϕ_i to the flow of the ϕ^n-vertex. The functions F_i depend on the external and loop momenta, p and q, respectively, as well as on the couplings G and Λ_n. The remaining p-dependence in (19) is projected out differently, depending on the quantity to be extracted. The momentum projection will be discussed below.

Summarising the present truncation, we consider the renormalisation group flow for the n-point correlation functions in a system of minimally-coupled gravity and matter. To this end, we employ a vertex expansion of the scale dependent effective action about a flat metric background to derive flow equations for the n-point correlators up to order three. The RG-invariant vertex dressing (7) allows to derive independently the flows of the momentum-independent couplings G, Λ_2 and Λ_3 as well as the momentum-dependent anomalous dimensions $\eta_h(p^2)$, $\eta_c(p^2)$, $\eta_\psi(p^2)$ and $\eta_\varphi(p^2)$. The couplings G and Λ_3 are computed from the transverse-traceless part of the graviton three-point function in the symmetric momentum configuration. Diffeomorphism invariant background couplings are computed from the solution of the dynamical couplings. Altogether, the present truncation yields the flow of the scale dependent parameters,

$$\{\bar{G}, \bar{\Lambda}, G, \Lambda_2, \Lambda_3, \eta_h(p^2), \eta_c(p^2), \eta_\psi(p^2), \eta_\varphi(p^2)\}\,. \tag{21}$$

III. FLOWS OF CORRELATION FUNCTIONS

The properties of the given theory are completely determined by the flows of the respective correlation functions. Thus, the latter parametrise the non-trivial interplay between gravity and matter. Matter is known to have a significant impact on the UV-behaviour of quantum gravity. On the other hand, graviton fluctuations can lead to strong correlations among matter fields. The resulting mutual dependencies play a crucial role for the flow of the complete system and are discussed separately in the following sections.

The computation of correlation functions described in this section involves the contraction of very large tensor structures. These contractions are computed with self-developed pattern-matching scripts. In this context we make use of the symbolic manipulation system *FORM* [57, 58].

A. Matter contributions to gravity flows

For the present analysis of quantum gravity, the gravity flows are extracted from the dynamical graviton two-point and three-point functions. The impact of matter manifests itself by matter loops in the diagrammatic representation of the flow. Figure 3 depicts these contributions for the flow of the graviton two-point function. The trace over the colour and flavour indices leads to weight factors of N_s and N_f for scalar and fermion loops, respectively. The matter contributions to $\mathrm{Flow}^{(hh)}$ are thus proportional to N_s or N_f. From $\mathrm{Flow}^{(hh)}$ we extract the flow of the graviton mass parameter defined as $M^2 := -2\Lambda_2$ and the graviton anomalous dimension η_h. This procedure is discussed in more detail in the following. A complete discussion can be found in [8].

$$\dot{\Gamma}^{(hh)}_{k,\mathrm{matter}} = N_s\left(-\frac{1}{2}\right. \quad + \quad \left.\right)$$
$$-2N_f\left(-\frac{1}{2}\right. \quad + \quad \left.\right)$$

FIG. 3. Diagrammatic representation of the matter induced flow of the graviton two-point function. Double, single and dashed lines represent graviton, fermion and scalar propagators respectively, filled circles denote dressed vertices. Crossed circles are regulator insertions.

From (7) we obtain an equation for the transverse-traceless graviton two-point function by contracting all external graviton legs with Π_{TT}. This leads to

$$\Gamma^{(hh)}_{\mathrm{TT}}(p^2) = \frac{1}{32\pi} Z_h(p^2)(p^2 + M^2)\,. \tag{22}$$

Taking a derivative with respect to renormalisation time t and dividing by $Z_h(p^2)$ yields

$$\mathrm{Flow}^{(hh)}_{\mathrm{TT}}(p^2) = \frac{1}{32\pi}\left(\partial_t M^2 - \eta_h(p^2)(p^2 + M^2)\right)\,. \tag{23}$$

The right hand side of the flow equation provides an expression for $\mathrm{Flow}^{(hh)}_{\mathrm{TT}}(p^2)$, which depends solely on the couplings and the anomalous dimensions. The resulting equation is evaluated at two different momentum scales p^2. Subtracting these two equations from each other allows for an unambiguous extraction of $\partial_t M^2$ and $\eta_h(p^2)$. We call this procedure bilocal momentum projection, it is applied for gravity in [1, 7, 8].

We extract the ghost anomalous dimension $\eta_c(p^2)$ from the transverse part of the ghost two-point function. The significance of the ghost contributions and details on their extraction are explained in [7, 8] and the explicit form is given in Appendix B.

The matter contributions to the flow for the graviton three-point function parametrise the impact of matter on the dynamical gravitational couplings g and λ_3. Figure 4 shows the matter contributions arising via loops in the diagrammatic representation. Again, the multiplicity of the matter-loops leads to contributions to $\mathrm{Flow}^{(hhh)}$ proportional to N_s and N_f. The flow for G and Λ_3 is extracted in a vein, similar to the extraction of η_h and $\partial_t M^2$ from the graviton two-point function. Projecting

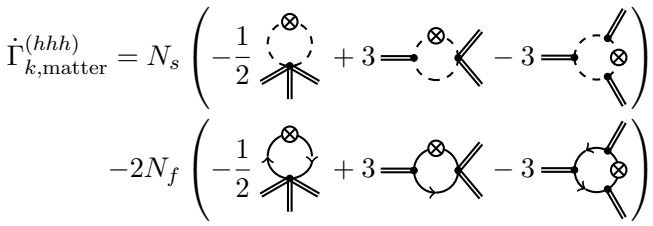

FIG. 4. Diagrammatic representation of the matter induced flow of the three-graviton vertex. Double, single and dashed lines represent graviton, fermion and scalar propagators respectively, filled circles denote dressed vertices. Crossed circles are regulator insertions. All diagrams are symmetrised with respect to the interchange of external momenta $\mathbf{p}$.

the flow of the three-graviton vertex on the transverse-traceless contributions of the classical tensor structures as described above and evaluating the kinematic configuration at the symmetric point as described in (17), yields equations of the type

$$\Gamma^{(hhh)}_{\mathrm{TT},i} = Z_h^{3/2}(p^2)\, G^{1/2}\left(\mathcal{N}_i\, p^2 + \mathcal{M}_i\, \Lambda_3\right) . \tag{24}$$

with $i = G, \Lambda$, for the projection on the tensor structures of G and Λ_3, respectively. The factors $\mathcal{N}_i$ and $\mathcal{M}_i$ arise from the tensor projection. They depend on the kinematic configuration and are given explicitly in Appendix A for the symmetric momentum configuration (17). Taking a scale derivative and rearranging leads to

$$\frac{2}{\sqrt{G}}\,\mathrm{Flow}^{(hhh)}_{\mathrm{TT},i} = 2\mathcal{M}_i\,\partial_t\Lambda_3 - \left[\eta_G + 3\eta_h(p^2)\right]\left(\mathcal{N}_i\, p^2 + \mathcal{M}_i\,\Lambda_3\right) , \tag{25}$$

with $\eta_G = -\partial_t \ln G$. Note, that (25) is structurally very similar to (23). For the extraction of the flows for the couplings G and Λ_3 we apply the bilocal momentum projection discussed before. Thus, we evaluate the flow of G at $p = k$ as well as at $p = 0$ and subtract both equations from each other. Since the term proportional to $\partial_t\Lambda_3$ in (25) is momentum independent, it drops out upon the subtraction thus leaving us an equation for $\partial_t G$. For the flow of Λ_3 it is then sufficient to evaluate (25) (with $i = \Lambda$) at vanishing external momentum $p = 0$. The resulting flow equations are identical to the ones in [1] and are given in Appendix A.

B. Gravity contributions to matter flows

In the matter sector, we consider the flows of the matter two-point functions. Since we do not admit matter self-interactions within the given truncation, these flows are driven solely by gravity-matter interactions. Furthermore, the matter fields are treated as massless, which is a good approximation for studies of the UV-behaviour of the theory. Consequently, the only quantities that are extracted here, are the matter anomalous dimensions. The effective action constructed from (10) is diagonal in both the colour and the flavour indices, i and k, respectively. We treat all scalars and all fermions on equal footing, providing them with one anomalous dimension for each of the field species, $\eta_\varphi(p^2)$ and $\eta_\psi(p^2)$, respectively. This allows for an extraction of the matter anomalous dimension from one representative field, since $\mathrm{Flow}^{(\varphi_k\varphi_l)} = \delta_{kl}\mathrm{Flow}^{(\varphi_k\varphi_k)}$ and $\mathrm{Flow}^{(\bar\psi_i\psi_j)} = \delta_{ij}\mathrm{Flow}^{(\bar\psi_i\psi_i)}$. Consequently, we drop the colour and flavour indices in the flows of the scalar and fermion two-point functions.

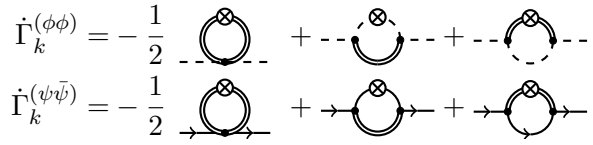

FIG. 5. Diagrammatic representation of the gravitationally induced flows of the matter-two-point-functions. Double, single and dashed lines represent graviton, fermion and scalar propagators respectively, filled circles denote dressed vertices. Crossed circles are regulator insertions.

Figure 5 depicts the flows of the matter two-point functions in diagrammatic representation which constitute the respective right hand sides of flow equation. From these flows we extract the matter anomalous dimensions. For the scalar fields the left hand side is given by

$$\mathrm{Flow}^{(\varphi\varphi)}(p^2) = -p^2\eta_\varphi(p^2)\,, \tag{26}$$

in complete analogy to the equation for the transverse-traceless graviton two-point function, (22). For the fermions we have the additional spinor structure which needs to be eliminated in order to obtain a Lorentz-scalar expression. The flow for the fermion two-point function reads

$$\mathrm{Flow}^{(\bar\psi\psi)}(p^2) = -i\not{p}\,\eta_\psi(p^2)\,. \tag{27}$$

By multiplying this expression with $\not{p}$ and taking the trace over the spinor indices we obtain an expression, which is identical to (22) and (26) up to prefactors, to wit

$$\mathrm{tr}(\not{p}\,\mathrm{Flow}^{(\bar\psi\psi)})(p^2) = -d\,i\,p^2\eta_\psi(p^2)\,. \tag{28}$$

Here d is the dimension of spinor space, which we set to $d = 4$ throughout. Since (22), (26) and (28) are of the same form, we apply the same bilocal momentum projection for the extraction of the respective momentum dependent anomalous dimensions. This crucial procedure is discussed in more detail in the next section.

C. Anomalous Dimensions

Each of the field species is equipped with an anomalous dimension $\eta_{\phi_i}(p^2)$. The latter are extracted from the flow

of the respective field's two point function. In the context of heat-kernel methods, the anomalous dimensions are often referred to as 'RG improvement' [20, 34, 51, 59]. In this work, they arise naturally from the truncation and as further improvement we keep an approximated momentum dependence of the anomalous dimension, similar to [1, 8].

The expressions (19), (26) and (28), together with the bilocal momentum projection lead to a coupled system of Fredholm integral equations for the anomalous dimensions $\vec{\eta}_\phi = (\eta_h, \eta_c, \eta_\psi, \eta_\varphi)$. The specific form of the latter is given in Appendix B. It can be written as

$$\vec{\eta}_\phi(p^2) = \vec{A}(p^2, G, M^2, \Lambda_3) + \vec{B}(p^2, G, M^2, \Lambda_3)[\vec{\eta}_\phi]\,, \tag{29}$$

where $\vec{A}$ and $\vec{B}$ are momentum-integral expressions. As the square brackets suggest, $\vec{B}$ is a functional of $\vec{\eta}_\phi(q^2)$. Equation (29) can be solved iteratively which is, however, computationally very expensive since it is a coupled system of four equations. In order to get a handle on the solution of (29), we evaluate the anomalous dimension in $\vec{B}$ at k^2 and move $\eta_\phi(k^2)$ in front of the integrals. This is a good approximation because all integrals of the type (19) are sharply peaked around $q = k$. This feature arises due to the factor of q^3 from the integral measure in $d = 4$ spherical coordinates. Since $\vec{B}$ is linear in $\vec{\eta}_\phi$, we can now write it as a matrix C multiplying the vector $\vec{\eta}_\phi(k^2)$. Hence, (29) simplifies to

$$\vec{\eta}_\phi(p^2) \approx \vec{A}(p^2, G, M^2, \Lambda_3) + C(p^2, G, M^2, \Lambda_3)\,\vec{\eta}_\phi(k^2)\,. \tag{30}$$

We now evaluate the latter equation at $p = k$ in order to obtain an expression for $\vec{\eta}_\phi(k^2)$. The result $\vec{\eta}_\phi(k^2)$ is substituted back into the momentum-dependent equation (30). This way, we obtain anomalous dimensions with an approximated momentum dependence. Note, that the latter approximation is considerably better than the assumption of momentum-independent anomalous dimensions, since we evaluate the functional dependence on $\vec{\eta}_\phi$ at the peak position of the integrals. In particular, this procedure allows for a distinction of $\vec{\eta}_\phi(k^2)$ and $\vec{\eta}_\phi(0)$, which is important since they both appear explicitly in the flow equations (C1), due to the bilocal momentum projection. We show in section IV A that our approximation is justified for the case without matter via comparison with the results from [1].

As an interesting fact, the scalar anomalous dimension $\eta_\varphi(p^2)$ vanishes for the given graviton gauge. Generally, the scalar anomalous dimension comprises a term which is proportional to the scalar mass and one mass-independent term. The latter vanishes for the used harmonic gauge. Obviously, the former term vanishes for massless scalars which we consider here, leaving us with a vanishing scalar anomalous dimension $\eta_\varphi(p^2) = 0$. Note that this is only the case for the scalar anomalous dimension in this particular gauge, for all other gauges $\eta_\varphi(p^2)$ is not equal to zero.

D. Anomalous dimensions and bounds for the generic class of regulators

As part of the truncation, we choose a generic class of regulators R_k^ϕ, that are proportional to the corresponding two-point function, i.e.

$$R_k^\phi(p^2) = \Gamma_k^{(\phi\phi)}(p^2) r_k^\phi(p^2)\Big|_{M^2=0}\,, \tag{31}$$

in momentum space, where $r_k^\phi(p^2)$ is the regulator shape function. Note, that the evaluation of the two-point function at $M^2 = 0$ ensures that only the momentum dependent part of the latter enters for the class of regulators defined by (31). Since the effective graviton mass M^2 is the only mass parameter in the present truncation the above definition implies that $\Gamma_k^{(\phi\phi)}(p^2)|_{M^2=0}$ is either the full two-point function $\Gamma_k^{(\phi\phi)}(p^2)$, or, in case of the graviton field, its momentum-dependent part, i.e. $\Gamma_{k,\mathrm{TT}}^{(hh)}(p^2)|_{M^2=0} = (32\pi)^{-1} Z_h(p^2) p^2$, see (22). This generic class covers the regulator choices in the literature, and implements the correct renormalisation group scaling of the effective action as discussed in [8, 41, 60]. It provides a RG-covariant infrared regularisation of the spectral values of the two-point function, and is hence called RG- or spectrally adjusted, [41, 60, 61]. It implies in particular, that the regulator is proportional to the corresponding field's wavefunction renormalisation via the dependence of R_k^ϕ on the two-point function. Thus, the present choice leads to closed equations in terms of the anomalous dimensions. However, for large η_ϕ the choice (31) leads to a peculiar RG-scaling of R_k^ϕ in the UV. From the path integral point of view one expects a UV scaling with

$$\lim_{k\to\infty} R_k^\phi(p) \sim \lim_{k\to\infty} Z_\phi k^i \to \infty\,, \tag{32}$$

for all momenta p. In (32) we have $i = 1$ for fermions and $i = 2$ for all other fields. Equation (32) entails that the regulator diverges in the UV, and the related momentum modes in the path integral are suppressed. Since the wavefunction renormalisation behaves like $Z_\phi \sim k^{-\eta_\phi}$ for large k, equation (32) is violated if the anomalous dimensions exceed the constraints

$$\eta_h < 2\,, \qquad \eta_c < 2\,, \qquad \eta_\varphi < 2\,, \qquad \eta_\psi < 1\,. \tag{33}$$

Hence, if one of the bounds in (33) is violated, the respective regulator vanishes in the UV. In the spirit of the above path integral picture this may imply a decrease of the effective cutoff scale for the respective field, and hence a flow towards the IR. Note however, that this is far from being clear from the flow equation itself. For example, with the regulator (31) the TT-component of the graviton propagator is proportional to

$$\frac{1}{Z_h(p^2)}\,\frac{1}{(p^2(1+r_h) + M^2)}\,, \tag{34}$$

which implies a spectral, RG-covariant regularisation of the momentum modes of the full propagator, as discussed above. We conclude that if the bounds in (33) are exceeded, the regulator may not suppress field modes in the UV properly. Indeed, if the anomalous dimension are large enough, this does not only lead to a decreasing regulator, but also $\partial_t R_k^\phi$ turns negative. This can be seen from the schematic expression

$$\partial_t R_k^\phi \sim Z_\phi(\dot{r}_k^\phi(p^2) - \eta_\phi r_k^\phi(p^2))\,. \tag{35}$$

The second term in equation (35) exceeds the first one for $p/k \to 0$ exactly at the critical values given in (33). Still, this is not sufficient to change the sign of the respective diagrams, which involves an integration over all momenta. However, for an even larger anomalous dimensions, $\eta_{\text{sign}} > 2$, the sign of the respective diagrams changes. In the path integral interpretation introduced above this change of sign signals the global change from a UV-flow to a IR- flow for the respective diagram. Naturally, this bound depends on the shape function of the regulator. For the present approximation, the first diagrams switch sign at $\eta_{\text{sign}} = 4$. This is already visible in the analytic, reduced, approximation derived later, see (C1). Note also, that the sign of diagrams does not change for Z_h-independent regulators. Accordingly, for $\eta_h > \eta_{\text{sign}}$ we have a regulator-dependence of the sign of diagrams, which has a qualitative impact on the physics under discussion. Hence, for $\eta_h > \eta_{\text{sign}}$ the present approximation breaks down completely. In the present work, however, we resort to the stricter, shape-function-independent bound (33).

In summary, it is clear that if the bounds (33) are violated, additional investigations of the regulator-dependence, and hence of the reliability of the present approximation are required. Note however, that small anomalous dimensions, that obey (33), do by no means guarantee the convergence of the results with respect to an extension of the truncation. Such a convergence study requires the inclusion of higher order operators and detailed regulator studies and is deferred to future work.

IV. RESULTS

In this section, the results of the above presented setups are displayed. As a main result, within the validity bounds for the chosen generic class of regulators, we do not find an upper limit for the numbers of scalars and fermions that are compatible with the asymptotic safety scenario.

For the analysis we employ regulators of the type given in (31) and use a Litim-type shape function [62] that is, $\sqrt{x}r(x) = (1-\sqrt{x})\theta(1-x)$ for fermions and $xr(x) = (1-x)\theta(1-x)$ for all other fields. We close the flow equations with the identification $\Lambda_5 = \Lambda_4 = \Lambda_3$. Furthermore, we work with the dimensionless quantities

$$g := Gk^2\,, \qquad \mu := M^2k^{-2}\,, \qquad \lambda_3 := \Lambda_3 k^{-2}\,. \tag{36}$$

A. Pure gravity

In order to study the UV behaviour of quantum gravity interacting with matter, we start from the UV fixed point of pure quantum gravity found in [1] and study the deformation of this particular fixed point by the matter content. To that end, we rederive the results for the pure gravity case with the approximated momentum dependence of the anomalous dimensions discussed in section III C. We compare these findings with the results in [1], where the full momentum dependence of the latter was considered. The fixed point values for the pure-gravity system in the present approximation read

$$(g^*, \mu^*, \lambda_3^*) = (0.62, -0.57, 0.095)\,, \tag{37a}$$

with the critical exponents θ_1, θ_2 and θ_3 given by

$$(\theta_{1/2}, \theta_3) = (-1.3 \pm 4.1\,i, 12)\,. \tag{37b}$$

These fixed point values are in agreement with [1] within an error of 6% (15% for the critical exponents). This justifies the approximations described in section III C. The deformation of the fixed point (37) is calculated while successively increasing the number of scalars and fermions, N_s and N_f, respectively. This way, we analytically continue the fixed point of the pure gravity system towards a theory of quantum gravity and matter, which contains N_s scalars and N_f fermions. Although N_f and N_s are (half-)integers in the physical sense, we treat them as continuous deformation parameters for this analysis. With this procedure we simulate the generic effect of gravity-matter interactions on gravity-theories. First, we analyse the influence of scalars and fermions separately before we briefly discuss combined system of both matter types.

B. Scalars

We first consider the case $N_f = 0$, $N_s > 0$, thus a theory of N_s scalars minimally coupled to gravity. Note again, that in the present approach, we neglect the influence of scalar self-interactions in the action (10). Detailed analyses of the potential impact of matter-matter couplings can be found in e.g. [63–65].

Before analysing the full numerical flow equations we try to anticipate the result from the analytic flow equations (C1) without anomalous dimensions. For $N_f = 0$, $N_s > 0$ and $\vec{\eta}_\phi = 0$ the latter equations read

$$\begin{aligned}
\dot{g} &= +2g + \beta_{g_{\text{Gravity}}} - \frac{43}{570\pi} g^2 N_s\,,\\
\dot{\mu} &= -2\mu + \beta_{\mu_{\text{Gravity}}} + \frac{1}{12\pi} g N_s\,,\\
\dot{\lambda}_3 &= -2\lambda_3 + \beta_{\lambda_{3,\text{Gravity}}} - \frac{1}{60\pi}\left(1 - \frac{43}{19}\lambda_3\right) g N_s\,.
\end{aligned} \tag{38}$$

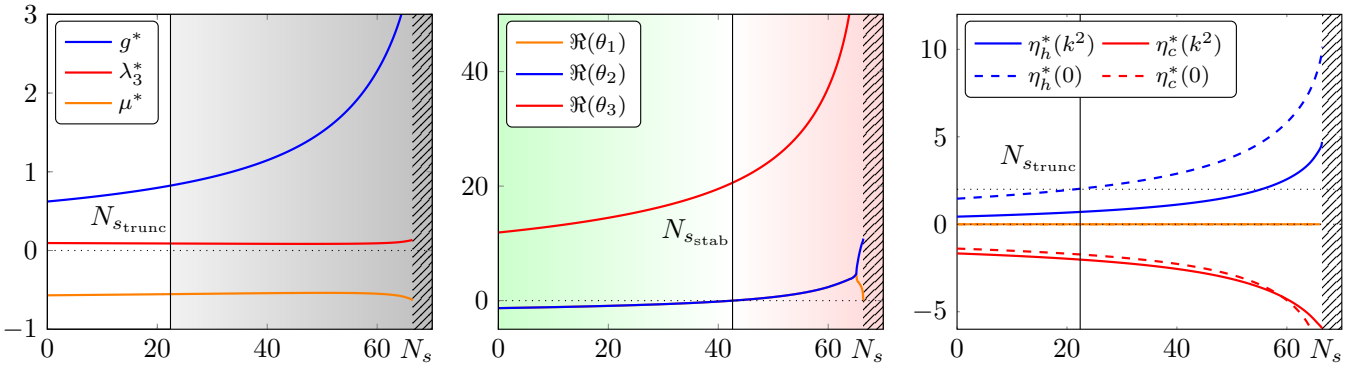

FIG. 6. Fixed point values (left), real parts of the critical exponents (middle), and the anomalous dimensions evaluated at $p = k$ and $p = 0$ (right) as functions of the number of scalars, N_s, respectively. The grey-shaded area in the left panel indicates where the regulator lies outside the reliability bounds defined in section III D due to a large graviton anomalous dimension (see right panel). The corresponding limiting number or scalars is given by $N_{s_{\rm trunc}}$. The hatched regions in all three panels correspond to the N_s-regime where the UV fixed point does not exist. The green and red areas in the middle panel denote the region where the fixed point exhibits UV-attractive direction and the region where it is fully repulsive, respectively. $N_{s_{\rm stab}}$ is the corresponding critical number. The colours of the curves in the middle panel indicate with which coupling of the left panel the corresponding eigenvector has the largest overlap. The anomalous dimension of the scalar η_φ (right panel) is zero due to the given graviton gauge.

In this set of equation we have split the running of the dimensionless couplings (g, μ, λ_3) into the canonical running, the contribution from graviton and ghost loops, and the contribution from scalar loops, in this ordering. In the following, we analyse whether the respective signs of the contributions potentially stabilise or destabilise the UV fixed point. A matter contribution to a given flow equation potentially destabilises the UV fixed point of the pure gravity system if it has the same sign as the canonical running. In this case, the contributions from graviton and ghost loops need to increase in to order to compensate for the matter contribution and, thus, allow for a gravity-matter fixed point. Conversely, if the canonical running and the matter contributions have the opposite sign we consider the matter contributions to potentially stabilise the fixed point. Further, we argue that the matter contribution to the running of μ has the largest impact on the flow compared to the other equations of the system (38).

Using the above notion, the scalar contribution to $\partial_t g$ potentially stabilises the fixed point, since the canonical running of g is positive and the N_s-dependent term has a negative sign. The positive sign of the N_s-term in $\partial_t \mu$ potentially destabilises the fixed point, since we have found $\mu^* < 0$ in the pure gravity case (see (37a)). Moreover, the contribution to $\partial_t \lambda_3$ is potentially destabilising, since we consider a positive and small λ_3 as in (37a). The behaviour is opposite for $\lambda_3 > 19/43$ and for $\lambda_3 < 0$.

We note that the flow equation for μ has the largest impact on the complete system (38). For one, that is because μ is the effective mass parameter of the graviton and, consequently, appears in all diagrams with graviton contributions in the loops. The second reason is that the fixed point value μ^* for the pure gravity system is close to -1. The μ-contributions to the flow equations generally take the form $(1+\mu)^{-n}$ with $n \geq 1$. Perturbations of μ are therefore strongly amplified if μ is close to -1. To see this we expand the general form of the μ-contributions around $-1/2$, namely $\mu = -1/2 + \epsilon$, which is approximately the fixed point value of the pure gravity system (see (37a)). The general form of the μ-contributions is now given by

$$\frac{1}{(1+\mu)^n} = \frac{2^n}{(1+2\epsilon)^n} \approx 2^n(1-2n\epsilon)\,, \tag{39}$$

which suggests that small perturbations of μ around $-1/2$ are amplified by a factor of $2n$ compared to contributions of order one which appear linearly in the numerators . Using a Litim-type regulator we obtain terms of the latter type in $\partial_t g$ up to $n = 5$. For these terms perturbations of μ around $-1/2$ are amplified by 10 compared to the linear quantities of order one. The impact of μ on the flow (38) becomes even larger, the closer μ is driven towards -1. For $\partial_t \lambda_3$ this argument is additionally supported by the smaller scalar contribution to $\partial_t \lambda_3$ compared to the respective contributions to $\partial_t g$ and $\partial_t \mu$. This also compensates for the fact that the fixed point value in the pure gravity case is $\lambda_3^* \approx 1/10$ and therefore not of order one. For these reasons, the scalar contributions in the flow of μ have the largest impact on the system (38).

In summary, we anticipate that the inclusion of scalar degrees of freedom potentially destabilises the UV fixed point. Hence, the gravity contributions in (38) must increase in order to compensate the destabilising N_s-contributions. This suggests that the couplings g^* and λ_3^* must increase with increasing N_s.

We now turn to the discussion of the UV fixed point for a varying number of scalars N_s in the full trunca-

tion. The left panel in Figure 6 shows the fixed point values of the dynamical quantities $(g^*, \mu^*, \lambda_3^*)$ of the system as a function of N_s. All fixed point values are continuous functions of the number of scalars in the regime $0 \leq N_s \leq 66.4 =: N_{s_{\max}}$. Outside this regime (hatched area), the fixed point disappears, thus, spoiling asymptotic safety of the corresponding theory. For $0 \leq N_s \leq 66.4 =: N_{s_{\max}}$, the fixed point value for the gravitational coupling g^* (blue curve) increases with increasing N_s, as conjectured from the analytic equations (38). Both, λ_3^* and μ^*, depicted in red and orange, respectively, remain almost constant, exhibiting only minor variations close to $N_{s_{\max}}$. The grey-shaded area in the left panel indicates where the regulator lies outside the reliability bounds defined in section III D due to a large graviton anomalous dimension (see right panel). The corresponding limiting number or scalars is given by $N_{s_{\text{trunc}}}$.

The middle panel in Figure 6 depicts the real parts of the critical exponents of the fixed point $(\Re(\theta_1), \Re(\theta_2), \Re(\theta_3))$ as functions of N_s. The colours of the curves are chosen such that the corresponding eigenvectors have the largest overlap with the coupling of the same colour in the left panel. All critical exponents increase with increasing N_s. The real part of the complex conjugate pair of eigenvalues $\Re(\theta_{1,2})$, represented by the blue and orange curves, changes sign at $N_{s_{\text{stab}}} = 42.6$. Consequently, the green and red areas correspond to N_s-regimes where the fixed point exhibits attractive directions and regimes where it is fully UV repulsive, respectively. In the regime $N_{s_{\text{stab}}} < N_s < N_{s_{\max}}$ the fixed point is fully UV-repulsive (red area). Furthermore, we observe that θ_3 takes large values for large N_s, which we see as further evidence for the insufficiency of the truncation in this regime [10, 21].

The right panel in Figure 6 shows the anomalous dimensions of all involved fields evaluated at the fixed point and at the peak of the loop integrals, $p = k$, as well as at vanishing momentum, $p = 0$. As discussed in section III C, the scalar anomalous dimension $\eta_\varphi(p^2)$ (orange curve) is zero for all p within the chosen gravity-gauge. In consequence, it does not appear explicitly in the legend of the panel. The graviton anomalous dimensions $\eta_h(k^2)$ and $\eta_h(0)$ both increase with increasing N_s due to the increase of g^*. At $N_{s_{\text{trunc}}} = 21.5$, $\eta_h(0)$ exceeds the critical value of $\eta_{h_{\text{crit}}} = 2$, discussed in section III C. Consequently, in the regime $N_{s_{\text{trunc}}} \leq N_s \leq N_{s_{\max}}$, the graviton anomalous dimension has exceeded the reliability bounds of the generic regulator class used here and we lose control over the suppression of graviton field modes by the regulator.

In summary, we draw the conclusion that within our truncation the inclusion of up to $N_s \approx 21$ scalars is consistent with the asymptotic safety scenario of quantum gravity. We also find that beyond this limit, our truncation exhibits a large graviton anomalous dimension beyond the critical value defined in (33). This suggests that the truncation should be improved in order to draw definite conclusions about the regime $N_s > N_{s_{\text{trunc}}}$. Therefore, the limits $N_{s_{\text{stab}}}$ and $N_{s_{\max}}$ found above, should be treated with caution as they could be artefacts of the present truncation.

The N_s-dependence of the couplings shown in Figure 6 is qualitatively different from that in [30, 34, 35]. This qualitative difference is also present in the fermion system discussed in the next section. A detailed comparison and evaluation of the reliability of the corresponding approximations is deferred to section V.

We conclude this analysis with a brief discussion of the bound η_{sign}. We have argued in section III C that for $\eta_h > \eta_{\text{sign}}$ the present approximation breaks down completely as the sign of diagrams is regulator-dependent. For the regulator used here, see section IV, we have $\eta_{\text{sign}} = 4$, see also (C1). Then the approximation breaks down for $N_{s_{\text{sign}}} \approx 65.4$ that is below but close to $N_{s_{\max}}$. As discussed in section III C, $N_{s_{\text{sign}}}$ signals the global change from a UV-flow to an IR-flow for the respective diagram and hence a mixed UV-IR–flow. Naturally, we expect the loss of the UV fixed point for such a flow.

C. Fermions

In this section we discuss the effect of minimally coupled fermions, thus $N_f > 0$ and $N_s = 0$ in our notation. As before, matter-self interactions are neglected.

Again, we first analyse the generic behaviour of the system of analytic flow equations (see Appendix C) with the simplification $\vec{\eta}_\phi = 0$. To that end, we again divide the flow into canonical running, gravity- and ghost-loop contributions, and matter-loop terms. Consequently, the latter equations read

$$\begin{aligned}
\dot{g} &= +2g + \beta_{g_{\text{Gravity}}} - \frac{3599}{11400\pi} g^2 N_f \,, \\
\dot{\mu} &= -2\mu + \beta_{\mu_{\text{Gravity}}} - \frac{8}{9\pi} g N_f \,, \\
\dot{\lambda}_3 &= -2\lambda_3 + \beta_{\lambda_{3,\text{Gravity}}} + \frac{1}{20\pi}\left(\frac{47}{7} + \frac{3599}{1140}\lambda_3\right) g N_f \,.
\end{aligned} \tag{40}$$

Using the notion introduced in the last section, we conclude that the fermionic contributions to $\partial_t g$ and $\partial_t \mu$ potentially stabilise the UV fixed point since they have signs opposite to the respective canonical running. The fermionic contribution to $\partial_t \lambda_3$, by contrast, is potentially destabilising. As we argued in the last section, the matter contribution to $\partial_t \mu$ is the most relevant one. Therefore, we expect that the fermion-gravity system remains stable under the increase of N_f. In particular, we expect smaller values for g^* for increasing N_f.

We turn now to the full numerical equations with momentum dependent anomalous dimensions. The left panel in Figure 7 shows the fixed point values of the dynamical quantities $(g^*, \mu^*, \lambda_3^*)$ as functions of the number of fermions N_f. The fixed point value of g decreases with increasing N_f and approaches $g^* \to 0$ asymptotically. At the same time, μ^* decreases with increasing N_f

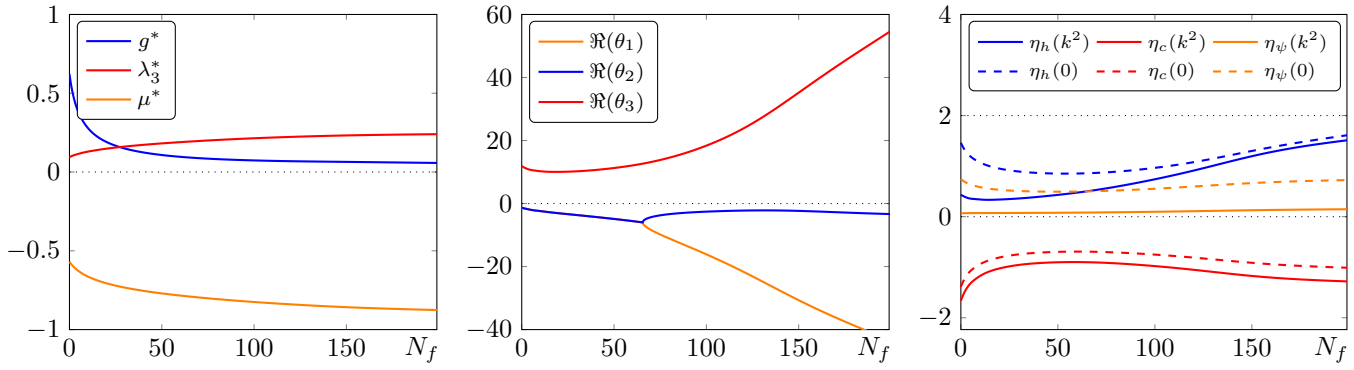

FIG. 7. Fixed point values (left), real parts of the critical exponents (middle), and the anomalous dimensions evaluated at $p = k$ and $p = 0$ (right) as functions of the number of fermions, N_f, respectively. The colours of the curves in the middle panel indicate with which coupling of the left panel the corresponding eigenvector has the largest overlap. All quantities remain well-behaved for any number of fermions. In particular, the fixed point stays attractive (middle panel) and the anomalous dimensions remain small (right panel).

and approaches $\mu^* \to \mu_{\text{pole}} = -1$ for $N_f \to \infty$. The fixed point value of λ_3 increases slightly with N_f and is driven towards an asymptotic value of $\lambda_3^* \approx 1/4$. It is important to note that the crucial negative sign of the fermionic contribution to $\partial_t \mu$, which is the same as in the analytic equations (40), gives rise to an interesting stabilising effect: Since we start with a negative μ^* for $N_f = 0$ the negative fermionic contribution in $\partial_t \mu$ drives μ^* towards more negative μ and therefore closer towards the propagator pole at $\mu_{\text{pole}} = -1$. This increases the contributions from graviton loops, which have the opposite sign compared to the fermionic terms to $\partial_t \mu$. Thus, the latter contributions cancel each other and the system settles at small values of g^*.

The middle panel in Figure 7 depicts the real parts of the critical exponents of the fixed point $(\Re(\theta_1), \Re(\theta_2), \Re(\theta_3))$ as functions of N_f. The colours are chosen such that the corresponding eigenvectors have the largest overlap with the coupling of the same colour in the left panel. The critical exponent of the repulsive direction θ_3 first decreases slightly and then increases to large values. The other two critical exponents $\theta_{1,2}$ form a complex conjugate pair with a decreasing real part until they reach $N_f = 65.5$. For $N_f > 65.5$ all critical exponents are real. In this regime, θ_1 decreases to smaller values, while θ_2 remains almost constant. The large absolute values of the critical exponents θ_1 and θ_3 indicate, similar to the scalar case, the necessity to extend the given truncation. Large critical exponents appear in particular for large numbers of fermions.

The right panel in Figure 7 shows the anomalous dimensions of the graviton, the ghost, and the fermion, η_h, η_c and η_ψ, respectively, evaluated at the fixed point. The anomalous dimensions are evaluated at the relevant momentum scales, $p = 0$ and $p = k$. Each anomalous dimension decreases at first and later increases slowly with increasing N_f. Nevertheless, all anomalous dimensions remain small. In particular, the graviton and the fermion anomalous dimension stay below their critical values $\eta_h < \eta_{h_{\text{crit}}} = 2$ and $\eta_\psi < \eta_{\psi_{\text{crit}}} = 1$, respectively.

In summary, we find an attractive UV fixed point for all numbers of fermions. Thus, all numbers of fermions are compatible with the asymptotic safety scenario. We also note that, in contradistinction to the scalar case, the anomalous dimensions stay sufficiently small even for a large number of fermions. However, the appearance of large critical exponents is seen as an indicator for the necessity to improve the truncation. In consequence, the impact of higher order operators will be studied in future work.

As in the scalar case we find that the N_f-dependence of the couplings shown in Figure 7 is qualitatively different from that in [30, 34, 35]. A detailed comparison and evaluation of the reliability of the corresponding approximations is deferred to section V.

D. Mixed Scalar-Fermion Systems

In this section, we consider the fixed point behaviour of mixed systems of scalars and fermions. The gravity-fermion system is stable for all N_f in the present approximation. In turn, the gravity-scalar system exceeds the bounds (33) far before the fixed point first becomes unstable and finally disappears. Thus, it is interesting to study the effect of a fixed number of fermions on the N_s-regime of validity. As discussed in section IV B, there exists a finite number of scalars $N_{s_{\text{trunc}}}$ for which η_h exceeds its critical value. In section IV C we observed that the inclusion of fermions leads to a decrease of g^*, which results in smaller anomalous dimensions. Therefore, we expect that the N_s-regime of validity is extended if we increase N_f.

In Figure 8 the fixed point value g^* is plotted as a function of N_s for different numbers of N_f. The vertical lines denote the numbers of scalars for which the graviton anomalous dimension exceeds its critical value in the UV. As displayed in the figure, the expected behaviour

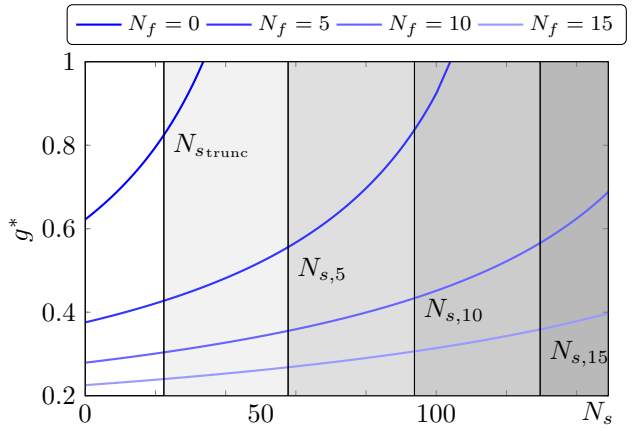

FIG. 8. Fixed point value g^* as a function of N_s for $N_f = 0, 5, 10, 15$. The vertical lines denote the numbers of scalars for which the graviton anomalous dimension exceeds its critical value in the UV, for the respective number of fermions.

for the combined systems is indeed realised. Thus, the increase of N_f lowers the fixed point value g^* and extends the N_s-regime of validity. For $N_f = 0$, 5, 10 and 15 the corresponding critical values $N_{s_{\mathrm{trunc}}}, N_{s,5}, N_{s,10}$ and $N_{s,15}$ are given by 21.5, 57.9, 93.8 and 129.6, respectively. The maximum number of scalars that defines the validity of the truncation increases almost linearly with N_f. Thus, every additional fermion stabilises the combined system such that ≈ 7.1 additional scalars are admitted. The ratio between these numbers suggests that fermions have a significantly stronger impact on the system than scalars. This is true for the complete truncation analysed here and can also be verified in the analytic equations by comparing the numerical values of the respective contributions (compare (38) and (40)). This imbalance between scalars and fermions was also observed in [34]. The increase of N_f also shifts the values of $N_{s_{\mathrm{sign}}}$ and $N_{s_{\mathrm{max}}}$ to larger values and extends the N_s-regime where a fixed point is found considerably. In summary, the inclusion of fermions stabilises the system and extends the N_s-regime of validity for the given truncation significantly.

E. Independence on the approximation in the gravity sector

We close this section with a brief discussion of the impact of the approximation in the pure gravity sector on our results. Interestingly, the results agree qualitatively for all approximations in the pure gravity sector used in the literature. This includes the standard ones in the background field approximation which are discussed in the next section. We also note that the fixed point for our truncated system is also present, if all anomalous dimension are set to zero. It is interesting to note, however, that for $N_s > 0$, $N_f = 0$ the fixed point vanishes already for $N_s \approx 45$ and therefore earlier than with anomalous dimensions. Thus, the anomalous dimensions stabilise the UV-behaviour of the system.

In order to combine the present matter contributions with the pure gravity systems in the geometrical framework [9], and with [8], we have to identify $\lambda_3 = \lambda_2 \equiv -\mu/2$. We find that the matter-contributions admit UV fixed points. Furthermore, we observe the same generic effect of scalars and fermions on the UV fixed point that was found for the present truncation. Hence, scalars drive the fixed point to larger values of g^*. while fermions lead to a decrease of g^* and μ^*, where μ^* approaches -1. In summary, our qualitative results are insensitive to the approximation in the pure gravity sector.

V. BACKGROUND COUPLINGS AND BACKGROUND-FIELD APPROXIMATION

It is left to study the stability of the results under a change of the approximation scheme in the matter sector. This is even more important as the N_s- and N_f-dependencies of the couplings shown in Figure 6 and Figure 7 are qualitatively different from those in [30, 34, 35]. The latter works use the background field approximation for the computation of the flows for the couplings, which are augmented with dynamical anomalous dimensions in [34, 35]. Hence, we compare the present system of dynamical couplings with the standard flows in the background field approximation.

In perturbatively renormalisable quantum field theories, like the Standard Model, the gauge invariant background couplings in the limit $k \to 0$ directly enter S-matrix computations. For $k \to 0$ the regulator, which typically depends on the background field, vanishes. For these reasons, these couplings are observables of the theory. In direct analogy, we call the diffeomorphism-invariant background couplings of quantum gravity also observables in the limit $k \to 0$. Note that these quantities have a clear physical interpretation only in the limit $k \to 0$. For $k > 0$, on the other hand, the background couplings depend inherently on the background-field content via the non-vanishing regulator. In this case, the couplings lose their clear physical meaning and their relation to observable quantities becomes unclear [1, 9].

In this section we use the notation $(g, \lambda_2, \lambda_3)$ for the dynamical couplings, where we reintroduced $\lambda_2 = -1/2\,\mu$. We also give a brief summary of the discussion in [9, 32, 37–41, 66, 67] on dynamical and background flows and the impact on the background field approximation: Standard approaches based on diffeomorphism invariant truncations use the background-field formalism for the definition of the truncated effective action. The corresponding flow equation, however, is not closed since it depends on the dynamical propagator. This is expressed schematically as

$$\dot{\Gamma}_k[\bar{g}, h] = F\left[\frac{\delta^2\Gamma_k[\bar{g}, h]}{\delta h^2}; \bar{g}\right], \tag{41}$$

where the separate dependence on $\bar{g}$ stems from the regulator. In order to close (41) the background-field approach amounts to the identification of the propagators of fluctuating and background-fields, i.e.,

$$\frac{\delta^2\Gamma_k[\bar{g},h]}{\delta h^2} \approx \frac{\delta^2\Gamma_k[\bar{g},h]}{\delta \bar{g}^2}\,. \tag{42}$$

The latter identification in known to pose severe problems in QCD, for more details see [8, 32]. However, at least for pure quantum gravity the approximation (42) seems to work rather well, leading to a reliable UV-behaviour of the theory. In the more elaborate geometrical-effective action approach [68, 69], the differences between fluctuating and background propagators are encoded in the (modified) Nielsen-Identities [40, 41]. In [9] the latter identities together with a minimally consistent extension to the Einstein-Hilbert truncation were used to derive flow equations for the dynamical couplings (g,λ) and the background couplings $(\bar{g},\bar{\lambda})$ in the absence of matter. In the geometrical approach the flow equations for the background couplings read schematically

$$\begin{aligned}\partial_t\left(\frac{k^2}{\bar{g}}\right) &= F_{R^1}(g,\lambda;N_s,N_f)\,,\\ \partial_t\left(\frac{\bar{\lambda}k^4}{\bar{g}}\right) &= F_{R^0}(g,\lambda;N_s,N_f)\,,\end{aligned} \tag{43}$$

for a theory with N_s scalars and N_f fermions. Note, that the right hand side of the latter equation only contains dynamical couplings. The dimensionful functions F_{R^1} and F_{R^0} correspond to the R^1 and R^0-terms of the required heat-kernel expansion, respectively. With the identification of background and dynamical couplings $(g,\lambda)=(\bar{g},\bar{\lambda})$, one retains the background-field approximation from the geometrical approach. Applying the derivatives in (43) leads us to

$$\begin{aligned}\frac{1}{\bar{g}}\left(2-\frac{\partial_t\bar{g}}{\bar{g}}\right) &= f_{R^1}(g,\lambda;N_s,N_f)\,,\\ \frac{\bar{\lambda}}{\bar{g}}\left(4+\frac{\partial_t\bar{\lambda}}{\bar{\lambda}}-\frac{\partial_t\bar{g}}{\bar{g}}\right) &= f_{R^0}(g,\lambda;N_s,N_f)\,,\end{aligned} \tag{44}$$

where $f_{R^i} := F_{R^i}\,k^{2(i-2)}$ is dimensionless. The equations (44) are now used to compare our flows for the dynamical couplings (g,λ_2,λ_3) with the standard background-field flows. Since both the standard background-field approximation and the geometrical effective action approach are based on diffeomorphism invariant truncations, they do not distinguish between the couplings of different-order graviton vertices. Hence, for the present analysis we set $\lambda_3 \equiv \lambda_2$ and identify the remaining couplings (g,λ_2) with the running dynamical gravitational coupling and the dynamical cosmological constant in the geometrical approach, $(g,\lambda)=(g,\lambda_2)$. We extract the expressions for f_{R^1} and f_{R^0} from the flow equations in [14, 34] reversing the identification of background and dynamical couplings. Explicit expressions for f_{R^i} are given in Appendix D.

In order to determine the fixed points of the flows (44), we set $\partial_t\bar{g}=\partial_t\bar{\lambda}=0$ and evaluate f_{R^i} at our fixed point values for the dynamical couplings, (g^*,λ_2^*). This way, we arrive at simple fixed point equations for the background couplings, to wit

$$\begin{aligned}\bar{g}^* &= \frac{2}{f_{R^1}(g^*,\lambda_2^*;N_s,N_f)}\\ \bar{\lambda}^* &= \frac{f_{R^0}(g^*,\lambda_2^*;N_s,N_f)}{2f_{R^1}(g^*,\lambda_2^*;N_s,N_f)}\,.\end{aligned} \tag{45}$$

The fixed points provided by the latter equations are compared to the results from flows in the standard background-field approximation [14, 34]. First of all, we note that the matter-terms in the flows of the dynamical couplings (g,λ_2) have opposite signs relative to the respective contributions to the flows of background couplings. This can be seen most easily in the analytical equations with $\vec{\eta}_\phi=0$ where the matter contributions to (g,λ_2) can be written as

$$\begin{aligned}\partial_t g &\sim -\frac{43}{570\pi}g^2N_s-\frac{3599}{11400\pi}g^2N_f\,,\\ \partial_t\lambda_2 &\sim -\frac{1}{24\pi}gN_s+\frac{4}{9\pi}gN_f\,.\end{aligned} \tag{46}$$

In [14, 34] the contributions to the flows of the background couplings $\bar{g}$ and $\bar{\lambda}$ read

$$\begin{aligned}\partial_t\bar{g} &\sim +\frac{1}{6\pi}\bar{g}^2N_s+\frac{1}{3\pi}\bar{g}^2N_f\\ \partial_t\bar{\lambda} &\sim +\frac{1}{12\pi}(3+2\bar{\lambda})\bar{g}N_s-\frac{1}{3\pi}(3-\bar{\lambda})\bar{g}N_f\,.\end{aligned} \tag{47}$$

For $\bar{\lambda}<3$ every single term in (46) and (47) carries the respective opposite sign.

Still, the signs of the matter contributions for the background flows are trivially the same. Accordingly, we expect the explicit N_s,N_f scalings in the flows of the background couplings to dominate the qualitative behaviour of the background fixed points. The implicit dependence of the fixed points (g^*,λ_2^*) on N_s,N_f is expected to be sub-leading, resulting in a similar behaviour of the fixed points of our background quantities and those from studies in background-field approximation.

A. Background fixed points in the full system

The left panel in Figure 9 shows the fixed point for the dynamical quantities (g,λ_2) (solid lines) and that of their corresponding background counterparts $(\bar{g},\bar{\lambda})$ (dashed lines) calculated from (45) as a function of N_s. The fixed point values of the background couplings have similar values compare to the fixed points for the dynamical couplings at $N_s=0$. However, both quantities

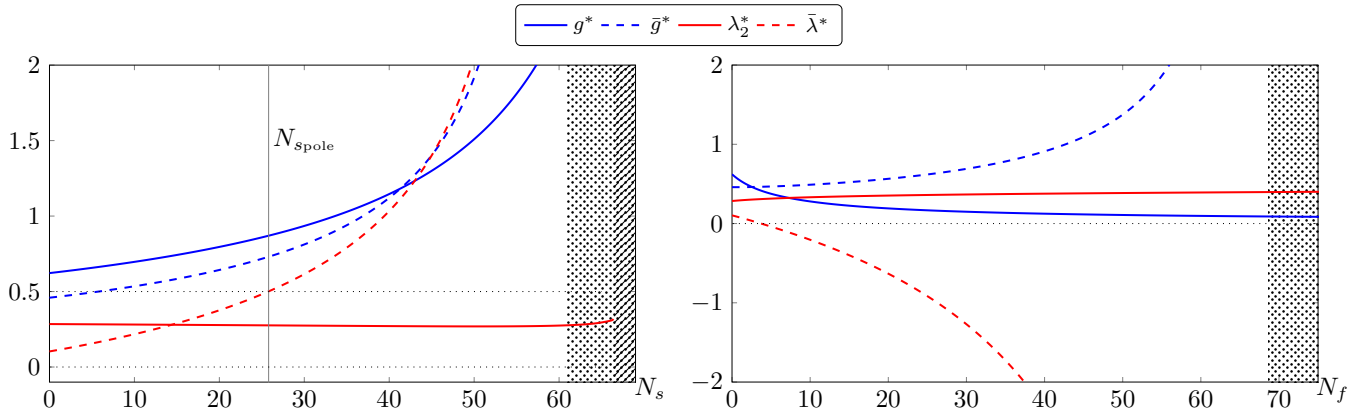

FIG. 9. Fixed point values of the dynamical couplings (g, λ_2) (solid lines) in comparison with their corresponding background counterparts $(\bar{g}, \bar{\lambda})$ (dashed lines) as functions of the number of scalars N_s (left panel) and the number of fermions N_f (right panel). The fixed point values of the background couplings diverge for $N_s = 60.8$ (left panel) and $N_f = 68.6$ (right panel). The dotted regions denote the regimes beyond the latter divergences. $N_{s_{\text{pole}}}$ denotes the number of scalars at which $\bar{\lambda}$ would run into the propagator pole, if the identification $\lambda_2 = \bar{\lambda}$, common in the background approximation, is applied.

evolve very differently under the inclusion of scalars. In particular, $\bar{g}$ and $\bar{\lambda}$ increase quickly with increasing N_s. At $N_{s_{\text{pole}}} = 25.8$, $\bar{\lambda}$ crosses the propagator pole, which is impossible in the background-field approximation. Here, however, we do not identify background and dynamical couplings, i.e. $\bar{\lambda} \neq \lambda_2$, and in consequence crossing of the pole does not pose a problem. The background couplings diverge for $N_s = 60.8$, resulting in an invalid fixed point for $N_s > 60.8$ (dotted area) . The latter divergence, however, is *not* present for the dynamical couplings. It merely results from the fact, that f_{R^1} becomes zero at this point, leading to divergent expressions for $(\bar{g}, \bar{\lambda})$ in (45). Consequently, the fixed point for the background couplings does in fact exist beyond $N_s = 60.8$ until the dynamical fixed point is lost (hatched area). Since f_{R^1} has, however, changed sign in this regime $\bar{g}^*$ is negative and, therefore, clearly unphysical.

The right panel in Figure 9 compares the fixed points for the dynamical couplings and the background couplings as a function of N_f. Starting at similar values at $N_f = 0$, the fixed point for the background couplings again exhibits a very different behaviour from that of the corresponding dynamical fixed points under the inclusion of fermions. While g^* decreases with increasing N_f, $\bar{g}$ increases strongly. Similarly, $\bar{\lambda}^*$ is quickly driven to large negative values, changing sign at $N_f = 3.7$, whereas the dynamical λ_2^* remains almost constant. The fixed point for the background quantities diverges for $N_f = 68.6$. The dotted region denotes the regime where the background fixed point is invalid. Again, the divergence appears only for the background quantities. The dynamical couplings remain well behaved for all N_f.

In summary, the fixed points for the background couplings behave very differently from their dynamical counterparts under the inclusion of matter fields. In particular, the latter exhibit divergences which are not present for the dynamical couplings. The dynamical couplings calculated in this work are the ones which are relevant for probing the consistency of gravity as a quantum field theory in the UV. Thus, the above analysis suggests that divergences or the disappearance of fixed points for the background couplings do not reflect actual divergences of the dynamical couplings. It is therefore indispensable, to distinguish between background and dynamical couplings in order to study the UV behaviour of quantum gravity, once matter fields are included.

B. Comparison to background fixed points in the literature

We now compare the fixed points for the background quantities, that we obtained from the equations (45), with the ones obtained from a background-field approximation as reported in [34]. In our analysis, we disregard the use of different regulators in the different approaches. Hence, we assume that the generic behaviour of the approaches is independent of this choice.

The left panel in Figure 10 depicts fixed points for background couplings as functions of N_s. The dotted curves represent fixed points of flows determined in background-field approximation in [34] (DEP) and the dashed curves denote our background couplings, which are calculated from the dynamical couplings (identical to the respective curves in Figure 9). The fixed point value for the gravitational coupling $\bar{g}^*_{\text{DEP}}$ increases with increasing N_s and eventually diverges at $N_s \approx 27$. For $N_s > 27$ no UV fixed point exists, which is indicated by the grey dotted area in the plot. Note, that due to the identification of background and dynamical couplings the graviton-propagator pole is located at $\bar{\lambda} = 0.5$. This limit cannot be intersected by $\bar{\lambda}^*_{\text{DEP}}$. In consequence, $\bar{\lambda}^*_{\text{DEP}}$ first increases but exhibits a characteristic kink at $N_s \approx 16$ and then decreases again until the fixed point

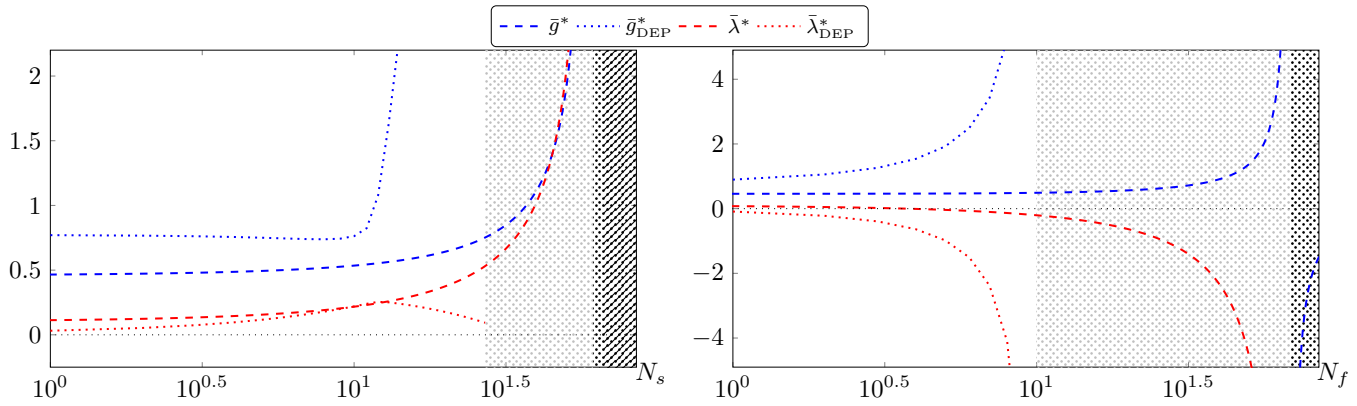

FIG. 10. Logarithmic plot of the fixed point values of the background field couplings $(\bar{g}, \bar{\lambda})$ as a function of the number of scalars N_s (left) and as a function of the number of fermions N_f (right) in comparison with results in background-field approximation from [34] (DEP). Our background couplings behave very similarly to the couplings in [34]. The grey and black-shaded area denote the regimes, where the fixed point for the couplings in [34] and for our couplings is lost, respectively.

ceases to exist at $N_s \approx 27$.

For small numbers of N_s, the fixed points from the background-field approach $(\bar{g}^*_{\rm DEP}, \bar{\lambda}^*_{\rm DEP})$ show a behaviour, which is similar to that of our background couplings $(\bar{g}^*, \bar{\lambda}^*)$. For larger values of N_s the value of $\bar{\lambda}^*_{\rm DEP}$ is driven closer to the propagator pole and the flow equations receive growing contributions from the graviton loops, which is not the case for our background couplings. Here, the implicit dependence of the fixed point on N_s is large and we observe large deviations between our background couplings and those in [34] in the regime $N_s \gtrsim 10$.

The right panel in Figure 10 depicts the fixed points for background couplings as functions of N_f. The notation for the curves in the right panel is the same as in the left one described above. The fixed point value $\bar{g}^*_{\rm DEP}$ strongly increases with increasing N_f and runs into a divergence for $N_f \approx 10$. For $N_f > 10$ the fixed point does not exist anymore, which is indicated by the grey dotted area in the plot. The value for $\bar{\lambda}^*_{\rm DEP}$ starts at small negative values and decreases quickly with increasing N_f until the fixed point ceases to exist at $N_f \approx 10$.

For small numbers of N_f, our background couplings $(\bar{g}^*, \bar{\lambda}^*)$ show again a similar behaviour to the fixed points in the background-field approximation. For larger N_f, we observe large deviations, though the generic behaviour of the fixed points is the same. An important common feature is the existence of a singularity for the fixed point for a finite number of fermions. As discussed in the previous section, this divergence has no influence on the asymptotic safety of the theory since it is clearly independent from the physical dynamical couplings. Again, the divergence of the background fixed point is due to the fact that f_{R^1} in (45) passes zero. Beyond this divergence the background fixed point still exists but has changed sign. This can be observed for $\bar{g}^*$ in the lower right corner of the right panel of Figure 10.

In summary, for sufficiently small $N_f, N_s \lesssim 10$ the couplings in the background-field approximation (DEP) behave similarly to the background-field couplings of the full dynamical system computed here. Note, that both computations show divergences in the background coupling for a finite number of scalars and fermions. These divergences are not reflected in the dynamical couplings and the current analysis strongly suggests their absence at $k = 0$. We conclude that the background-field approximation provides an adequate qualitative picture of the behaviour of the physical background couplings for $N_f, N_s \lesssim 10$. The relevant quantities for studies of the UV behaviour of quantum gravity are, however, the dynamical couplings. In turn, for $N_f, N_s \gtrsim 10$ the background field approximation fails, and it is necessary to compute dynamical flows and couplings.

VI. SUMMARY

We have presented the first genuine calculation of dynamical gravitational couplings based on a vertex flow in gravity-matter systems with an arbitrary number of scalars and fermions. We have calculated the matter contributions to the dynamical graviton two- and three-point functions and included momentum-dependent gravity and matter anomalous dimensions. The UV behaviour of the resulting theory has been analysed under the influence of N_s scalars and N_f fermions.

In the scalar sector the increase of N_s leads to an increasing Newton's coupling at the UV fixed point and thus to a strengthening of graviton fluctuations at high energies. For large numbers of scalars $N_s > 21.5$ the present generic class of regulators violates the bounds (33) due to a large graviton anomalous dimension, i.e. $\eta_h > 2$ in this regime. Deep in this regime the UV fixed point first becomes repulsive and finally is lost, which requires further investigation.

In the fermion sector the UV fixed point exists and is stable for all N_f. Also, all fixed point values re-

main small, and the anomalous dimensions stay below the bounds (33), i.e. $\eta_h, \eta_c, \eta_\varphi < 2$ and $\eta_\psi < 1$, for all N_f. Similar to the scalar case the increase of N_f enhances graviton fluctuations. Here however, the enhancement is due to the shift of the graviton-mass parameter towards the propagator pole.

In summary, we always find an attractive UV fixed point in the presence of a general number of scalars and fermions within the validity bounds for the generic class of regulators used here. Finally we have discussed and embedded previous results in the literature within our extended setting. In particular we have also compared the present results within the full dynamical system to results that partially rely on the background field approximation. Interestingly, we find the signs of the matter contributions to the flows of our dynamical couplings to be opposite to those of flows in background-field approximation. This is in sharp contrast to the pure gravity flows whose signs agree in all approximations. We have also computed the fixed points of the background couplings in the present approach. We have shown that the latter agree qualitatively with the fixed point couplings in in the background-field approximation for $N_f, N_s \lesssim 10$. In turn, for $N_f, N_s \gtrsim 10$ the background field approximation fails, and it is necessary to compute dynamical flows and couplings.

Currently, we extend the present work to vector fields as well as to improved approximations. This includes approximations that are not sensitive to the validity bounds for the generic class of regulators used here related to the size of the anomalous dimensions as well as including higher orders in the curvature scalar R.

Acknowledgements We thank N. Christiansen, A. Eichhorn, K. Falls, H. Gies, T. Henz, R. Percacci, A. Rodigast and C. Wetterich for discussions. MR acknowledges funding from IMPRS-PTFS. This work is supported by EMMI and by ERC-AdG-290623.

Appendix A: Flow of the Three-Point Function

In section II and in section III A we discussed the projection and the flow of the graviton three-point function. Here we provide the explicit form of the projection operators, and the corresponding projected flow equations. In the three-step procedure outlined in section II we presented a way to construct two projection operators for the three-point function. From the momentum-independent part of $\mathcal{T}^{(3)}$ we obtained a projection operator for $\partial_t \Lambda_3$, which we call Π_{Λ_3}. In turn, the corresponding projection operator for $\partial_t G$, Π_G, was constructed from the momentum dependent part of $\mathcal{T}^{(3)}$. In a multi-index notation, Π_G (in the symmetric momentum configuration) and Π_{Λ_3} are given by

$$\Pi_G^{ABC} = \Pi_{\text{TT}}^{AA'}(p_1^2)\Pi_{\text{TT}}^{BB'}(p_2^2)\Pi_{\text{TT}}^{CC'}(p_3^2)\frac{\mathcal{T}^{(3)}_{A'B'C'}(\mathbf{p};0)}{p_1^2}\,, \tag{A1}$$

$$\Pi_{\Lambda_3}^{ABC} = \Pi_{\text{TT}}^{AA'}(p_1^2)\Pi_{\text{TT}}^{BB'}(p_2^2)\Pi_{\text{TT}}^{CC'}(p_3^2)\mathcal{T}^{(3)}_{A'B'C'}(0;1)\,, \tag{A2}$$

where A, B and C are multi-indices, e.g. $A = \mu\nu$. Contracting $\Gamma_k^{(hhh)}$ with these objects leads to scalar expressions, which we call $\Gamma^{(hhh)}_{\text{TT},G}$ and $\Gamma^{(hhh)}_{\text{TT},\Lambda}$, respectively. The latter are given schematically in equation (24) and read explicitly

$$\Gamma^{(hhh)}_{\text{TT},G}(p^2) = G^{1/2}\frac{Z_h^{3/2}(p^2)}{(32\pi)^2}\left(\frac{171}{32}p^2 - \frac{9}{4}\Lambda_3\right)\,, \tag{A3}$$

$$\Gamma^{(hhh)}_{\text{TT},\Lambda}(0) = G^{1/2}\frac{Z_h^{3/2}(0)}{(32\pi)^2}\frac{80}{3}\Lambda_3\,, \tag{A4}$$

where the subscript G and Λ refer to the different projections schemes as described in the equations (A1) and (A2). From these equations we take a scale derivative and divide by the appropriate wavefunction renormalisation, i.e. $Z_h^{3/2}(p^2)$ for equation (A3) and $Z_h^{3/2}(0)$ for equation (A4). Afterwards (A3) is evaluated at $p = k$ as well as $p = 0$. The respective results are subtracted from each other. With the usual dimensionless quantities introduced in (36) this leads to the flow equations

$$\begin{aligned}\dot{g} =& 2g + 3\eta_h(k^2)g - \frac{24}{19}\left(\eta_h(k^2) - \eta_h(0)\right)\lambda_3\, g \\ &+ \frac{64}{171}\frac{(32\pi)^2\sqrt{g}}{k}\left(\text{Flow}^{(hhh)}_{\text{TT},G}(k^2) - \text{Flow}^{(hhh)}_{\text{TT},G}(0)\right)\,,\end{aligned} \tag{A5}$$

$$\begin{aligned}\dot{\lambda}_3 =& -2\lambda_3 + \frac{3}{2}\eta_h(0)\lambda_3 + \frac{1}{2}(2g - \dot{g})\frac{\lambda_3}{g} \\ &+ \frac{3}{80}\frac{(32\pi)^2}{\sqrt{g}k}\text{Flow}^{(hhh)}_{\text{TT},\Lambda}(0)\,.\end{aligned} \tag{A6}$$

Note, that prefactors such as $\frac{24}{19}$ or $\frac{64}{171}$ depend on the kinematic configuration. The present flow equations are evaluated for the symmetric momentum configuration, see (17). The prefactors in front of Flow also depend on the norm of the projection operators. The present numbers are obtained with unnormalised transverse-traceless projection operators, i.e. $\Pi_{\text{TT}} \circ \Pi_{\text{TT}} = 5$. These equations do not have an analytic form. To obtain analytic equations, a derivative projection is necessary, but this is less accurate in capturing the momentum dependence of the flow, see Appendix C.

Appendix B: Anomalous Dimensions

The anomalous dimensions obey a system of coupled Fredholm integral equations. The latter is given by

$$\eta_h(p^2) = 32\pi\frac{\text{Flow}^{(hh)}_{\text{TT}}(-M^2) - \text{Flow}^{(hh)}_{\text{TT}}(p^2)}{p^2 + M^2}[\vec{\eta}_\phi]\,,$$

$$\eta_c(p^2) = -\frac{\text{Flow}^{(\bar{c}c)}(p^2)}{p^2}[\eta_h, \eta_c]\,,$$

$$\eta_\psi(p^2) = i\frac{\text{tr}(\not{p}\text{Flow}^{(\bar{\psi}\psi)})(p^2)}{d\,p^2}[\eta_h, \eta_\psi]\,,$$

$$\eta_\varphi(p^2) = -\frac{\text{Flow}^{(\varphi\varphi)}(p^2)}{p^2}[\eta_h, \eta_\varphi]\,. \tag{B1}$$

The squared brackets denote functional dependencies on the respective anomalous dimensions. The content of the brackets also indicates which fields run in the loop of corresponding two-point function. We approximate the equations (B1) by evaluating the anomalous dimension at the momentum scale $p = k$, see section III C.

Appendix C: Analytic Flow Equations

Throughout this work we have used the full numerical flow equations to compute the UV fixed points. Nevertheless, we derived analytic flow equations, which are, however, less accurate in capturing the momentum dependence of the flow [1]. To obtain analytic flow equations we need to employ

- a Litim-type regulator,
- the momentum approximation of the anomalous dimension from section III C in each loop integral,
- a derivative projection for $\partial_t g$ instead of the usual bilocal projection (for bilocal projection see Appendix A).

The latter implies the following: As usual, we take a scale derivative of equation (A3) and divide by $Z_h^{3/2}(p^2)$ and p^2. Then, we take another derivative, this time with respect to p^2 and evaluate the result at $p = 0$. Now, the loop integration can be performed analytically. The resulting analytic equations are

$$\begin{aligned}
\dot{g} = &\left(2 + 3\eta_h(0) - \frac{24}{19}\eta_h'(0)\lambda_3\right) g \\
&+ \frac{g^2}{\pi}\left(-\frac{47(6-\eta_h(k^2))}{114(\mu+1)^2} + \frac{\left(472(6-\eta_h(k^2)) - 360(4-\eta_h(k^2))\lambda_3\right)\lambda_4 - 240(6-\eta_h(k^2))\lambda_3 + 45(8-\eta_h(k^2))}{342(\mu+1)^3}\right. \\
&\quad + \frac{16(1-3\lambda_3)\lambda_4}{19(\mu+1)^4} + \frac{25920(4-\eta_h(k^2))\lambda_3^3 + 3380(6-\eta_h(k^2))\lambda_3^2 - 1860(8-\eta_h(k^2))\lambda_3 + 147(10-\eta_h(k^2))}{1710(\mu+1)^4} \\
&\quad \left. + 2\frac{2336\lambda_3^3 - 3640\lambda_3^2 + 1780\lambda_3 - 299}{285(\mu+1)^5} - \frac{53(10-\eta_c(k^2))}{190} + \frac{48}{19}\right) \\
&+ N_f\frac{g^2}{\pi}\left(-\frac{521(6-\eta_\psi(k^2))}{17100} - \frac{3(5-\eta_\psi(k^2))}{152} - \frac{13}{380}\right) \\
&+ N_s\frac{g^2}{\pi}\left(\frac{10-\eta_\varphi(k^2)}{1140} - \frac{8}{95}\right)\,,
\end{aligned}$$

$$\begin{aligned}
\dot{\lambda}_3 = &\left(-1 + \frac{3}{2}\eta_h(0) - \frac{\dot{g}}{2g}\right)\lambda_3 \\
&+ \frac{g}{\pi}\left(\frac{8-\eta_h(k^2) - 4(6-\eta_h(k^2))\lambda_5}{8(\mu+1)^2} + \frac{(-16(6-\eta_h(k^2))\lambda_3 + 3(8-\eta_h(k^2)))\lambda_4}{6(\mu+1)^3}\right. \\
&\quad \left. + \frac{80(6-\eta_h(k^2))\lambda_3^3 - 120(8-\eta_h(k^2))\lambda_3^2 + 72(10-\eta_h(k^2))\lambda_3 - 11(12-\eta_h(k^2))}{240(\mu+1)^4} + \frac{12-\eta_c(k^2)}{10}\right) \\
&+ N_f\frac{g}{\pi}\left(\frac{8-\eta_\psi(k^2)}{224} - \frac{7-\eta_\psi(k^2)}{56} + \frac{17(6-\eta_\psi(k^2))}{240}\right) \\
&+ N_s\frac{g}{\pi}\left(\frac{12-\eta_\varphi(k^2)}{480} - \frac{10-\eta_\varphi(k^2)}{80} + \frac{8-\eta_\varphi(k^2)}{96}\right)\,,
\end{aligned}$$

$$
\begin{aligned}
\dot{\mu} =& \Big(-2 + \eta_h(0) \Big) \mu \\
&+ \frac{g}{\pi} \left(\frac{8(6-\eta_h(k^2))\lambda_4 - 3(8-\eta_h(k^2))}{12(\mu+1)^2} + \frac{320(6-\eta_h(k^2))\lambda_3^2 - 120(8-\eta_h(k^2))\lambda_3 + 21(10-\eta_h(k^2))}{180(\mu+1)^3} \right. \\
&\qquad \left. - \frac{10-\eta_c(k^2)}{5} \right) \\
&+ N_f \frac{g}{\pi} \left(\frac{7-\eta_\psi(k^2)}{63} - \frac{6-\eta_\psi(k^2)}{6} \right) \\
&+ N_s \frac{g}{\pi} \left(\frac{10-\eta_\varphi(k^2)}{120} \right) .
\end{aligned} \tag{C1}
$$

Appendix D: Background Quantities

The functions f_{R^i}, which are discussed in section V, are extracted from [34]. In our case they read

$$
\begin{aligned}
f_{R^0}(g,\lambda,N_s,N_f) =& \frac{1}{48\pi} \left(\frac{20(6-\eta_h(k^2))}{1-2\lambda} - 16(6-\eta_c(k^2)) + 2(6-\eta_\varphi(k^2))N_s - 8(6-\eta_\psi(k^2))N_f \right) , \\
f_{R^1}(g,\lambda,N_s,N_f) =& \frac{1}{48\pi} \left(\frac{52(4-\eta_h(k^2))}{1-2\lambda} + 40(4-\eta_c(k^2)) - 2(4-\eta_\varphi(k^2))N_s - 4(4-\eta_\psi(k^2))N_f \right) .
\end{aligned} \tag{D1}
$$

In order to obtain the functions in equation (D1), we reversed the identification of background and dynamical quantities and replaced $\eta_\phi \to \eta_\phi(k^2)$ in order to evaluate the anomalous dimension at the values, where the integrals are peaked. Note, that the functions f_{R^i} depend on the dynamical gravitational coupling g only via the anomalous dimensions.

[1] N. Christiansen, B. Knorr, J. Meibohm, J. M. Pawlowski, and M. Reichert, Phys. Rev. **D92**, 121501 (2015), arXiv:1506.07016 [hep-th].
[2] S. Weinberg, General Relativity: An Einstein centenary survey, Eds. Hawking, S.W., Israel, W; Cambridge University Press , 790 (1979).
[3] M. Reuter, Phys. Rev. **D57**, 971 (1998), arXiv:hep-th/9605030.
[4] C. Wetterich, Phys.Lett. **B301**, 90 (1993).
[5] W. Souma, Prog.Theor.Phys. **102**, 181 (1999), arXiv:hep-th/9907027 [hep-th].
[6] M. Reuter and F. Saueressig, Phys. Rev. **D65**, 065016 (2002), arXiv:hep-th/0110054 [hep-th].
[7] N. Christiansen, D. F. Litim, J. M. Pawlowski, and A. Rodigast, Phys.Lett. **B728**, 114 (2014), arXiv:1209.4038 [hep-th].
[8] N. Christiansen, B. Knorr, J. M. Pawlowski, and A. Rodigast, Phys. Rev. **D93**, 044036 (2016), arXiv:1403.1232 [hep-th].
[9] I. Donkin and J. M. Pawlowski, (2012), arXiv:1203.4207 [hep-th].
[10] K. Falls, D. F. Litim, K. Nikolakopoulos, and C. Rahmede, (2014), arXiv:1410.4815 [hep-th].
[11] O. Lauscher and M. Reuter, Phys. Rev. **D66**, 025026 (2002), arXiv:hep-th/0205062.
[12] A. Codello and R. Percacci, Phys. Rev. Lett. **97**, 221301 (2006), arXiv:hep-th/0607128.
[13] A. Codello, R. Percacci, and C. Rahmede, Int. J. Mod. Phys. **A23**, 143 (2008), arXiv:0705.1769 [hep-th].
[14] A. Codello, R. Percacci, and C. Rahmede, Annals Phys. **324**, 414 (2009), arXiv:0805.2909 [hep-th].
[15] P. F. Machado and F. Saueressig, Phys. Rev. **D77**, 124045 (2008), arXiv:0712.0445 [hep-th].
[16] D. Benedetti, P. F. Machado, and F. Saueressig, Mod. Phys. Lett. **A24**, 2233 (2009), arXiv:0901.2984 [hep-th].
[17] A. Eichhorn, H. Gies, and M. M. Scherer, Phys. Rev. **D80**, 104003 (2009), arXiv:0907.1828 [hep-th].

[18] E. Manrique, S. Rechenberger, and F. Saueressig, Phys.Rev.Lett. **106**, 251302 (2011), arXiv:1102.5012 [hep-th].
[19] S. Rechenberger and F. Saueressig, Phys.Rev. **D86**, 024018 (2012), arXiv:1206.0657 [hep-th].
[20] A. Codello, G. D'Odorico, and C. Pagani, Phys. Rev. **D89**, 081701 (2014), arXiv:1304.4777 [gr-qc].
[21] K. Falls, D. Litim, K. Nikolakopoulos, and C. Rahmede, (2013), arXiv:1301.4191 [hep-th].
[22] K. Falls, JHEP **01**, 069 (2016), arXiv:1408.0276 [hep-th].
[23] K. Falls, Phys. Rev. **D92**, 124057 (2015), arXiv:1501.05331 [hep-th].
[24] H. Gies, B. Knorr, and S. Lippoldt, Phys. Rev. **D92**, 084020 (2015), arXiv:1507.08859 [hep-th].
[25] M. Niedermaier and M. Reuter, Living Rev.Rel. **9**, 5 (2006).
[26] R. Percacci, In *Oriti, D. (ed.): Approaches to quantum gravity* 111-128 (2007), arXiv:0709.3851 [hep-th].
[27] D. F. Litim, Phil.Trans.Roy.Soc.Lond. **A369**, 2759 (2011), arXiv:1102.4624 [hep-th].
[28] M. Reuter and F. Saueressig, New J. Phys. **14**, 055022 (2012), arXiv:1202.2274 [hep-th].
[29] D. Dou and R. Percacci, Class. Quant. Grav. **15**, 3449 (1998), arXiv:hep-th/9707239 [hep-th].
[30] R. Percacci and D. Perini, Phys. Rev. **D67**, 081503 (2003), arXiv:hep-th/0207033.
[31] R. Percacci and D. Perini, Phys. Rev. **D68**, 044018 (2003), arXiv:hep-th/0304222.
[32] S. Folkerts, D. F. Litim, and J. M. Pawlowski, Phys.Lett. **B709**, 234 (2012), arXiv:1101.5552 [hep-th].
[33] P. Donà and R. Percacci, Phys. Rev. **D87**, 045002 (2013), arXiv:1209.3649 [hep-th].
[34] P. Donà, A. Eichhorn, and R. Percacci, Phys.Rev. **D89**, 084035 (2014), arXiv:1311.2898 [hep-th].
[35] P. Donà, A. Eichhorn, and R. Percacci, *Proceedings, Satellite Conference on Theory Canada 9*, Can. J. Phys. **93**, 988 (2015), arXiv:1410.4411 [gr-qc].
[36] K.-y. Oda and M. Yamada, (2015), arXiv:1510.03734 [hep-th].
[37] J. M. Pawlowski, Acta Phys.Slov. **52**, 475 (2002).
[38] D. F. Litim and J. M. Pawlowski, JHEP **0209**, 049 (2002), arXiv:hep-th/0203005 [hep-th].
[39] D. F. Litim and J. M. Pawlowski, Phys.Lett. **B546**, 279 (2002), arXiv:hep-th/0208216 [hep-th].
[40] J. M. Pawlowski, (2003), arXiv:hep-th/0310018 [hep-th].
[41] J. M. Pawlowski, Annals Phys. **322**, 2831 (2007), arXiv:hep-th/0512261 [hep-th].
[42] V. Branchina, K. A. Meissner, and G. Veneziano, Phys.Lett. **B574**, 319 (2003), arXiv:hep-th/0309234 [hep-th].
[43] M. Demmel, F. Saueressig, and O. Zanusso, Annals Phys. **359**, 141 (2015), arXiv:1412.7207 [hep-th].
[44] M. Demmel and A. Nink, Phys. Rev. **D92**, 104013 (2015), arXiv:1506.03809 [gr-qc].
[45] M. Safari, (2015), arXiv:1508.06244 [hep-th].
[46] E. Manrique and M. Reuter, Annals Phys. **325**, 785 (2010), arXiv:0907.2617 [gr-qc].
[47] E. Manrique, M. Reuter, and F. Saueressig, Annals Phys. **326**, 463 (2011), arXiv:1006.0099 [hep-th].
[48] M. Reuter and C. Wetterich, Nucl. Phys. **B417**, 181 (1994).
[49] U. Ellwanger, Z. Phys. **C62**, 503 (1994), arXiv:hep-ph/9308260 [hep-ph].
[50] T. R. Morris, Int. J. Mod. Phys. **A9**, 2411 (1994), arXiv:hep-ph/9308265.
[51] A. Eichhorn and H. Gies, Phys. Rev. **D81**, 104010 (2010), arXiv:1001.5033 [hep-th].
[52] C. S. Fischer and J. M. Pawlowski, Phys. Rev. **D80**, 025023 (2009), arXiv:0903.2193 [hep-th].
[53] H. A. Weldon, Phys. Rev. **D63**, 104010 (2001), arXiv:gr-qc/0009086 [gr-qc].
[54] H. Gies and S. Lippoldt, Phys.Rev. **D89**, 064040 (2014), arXiv:1310.2509 [hep-th].
[55] S. Lippoldt, Phys. Rev. **D91**, 104006 (2015), arXiv:1502.05607 [hep-th].
[56] D. F. Litim and J. M. Pawlowski, Phys.Lett. **B435**, 181 (1998), arXiv:hep-th/9802064 [hep-th].
[57] J. Kuipers, T. Ueda, J. A. M. Vermaseren, and J. Vollinga, Comput. Phys. Commun. **184**, 1453 (2013), arXiv:1203.6543 [cs.SC].
[58] J. A. M. Vermaseren, (2000), arXiv:math-ph/0010025 [math-ph].
[59] K. Groh and F. Saueressig, J. Phys. **A43**, 365403 (2010), arXiv:1001.5032 [hep-th].
[60] J. M. Pawlowski, Int.J.Mod.Phys. **A16**, 2105 (2001).
[61] H. Gies, Phys. Rev. **D66**, 025006 (2002), arXiv:hep-th/0202207 [hep-th].
[62] D. F. Litim, Phys.Lett. **B486**, 92 (2000), arXiv:hep-th/0005245 [hep-th].
[63] A. Eichhorn and H. Gies, New J. Phys. **13**, 125012 (2011), arXiv:1104.5366 [hep-th].
[64] A. Eichhorn, Phys. Rev. **D86**, 105021 (2012), arXiv:1204.0965 [gr-qc].
[65] T. Henz, J. M. Pawlowski, A. Rodigast, and C. Wetterich, Phys. Lett. **B727**, 298 (2013), arXiv:1304.7743 [hep-th].
[66] I. H. Bridle, J. A. Dietz, and T. R. Morris, JHEP **03**, 093 (2014), arXiv:1312.2846 [hep-th].
[67] J. A. Dietz and T. R. Morris, JHEP **04**, 118 (2015), arXiv:1502.07396 [hep-th].
[68] G. Vilkovisky, Nucl.Phys. **B234**, 125 (1984).
[69] B. S. DeWitt, Quantum Field Theory and Quantum Statistics, Vol. 1, Batalin, I.A. (Ed.) et al. , 191 (1988).